Journal of Hydrology 581 (2020) 124430

Contents lists available at ScienceDirect

Journal of Hydrology

journal homepage: www.elsevier.com/locate/jhydrol

Research papers

Large wood (LW) 3D accumulation mapping and assessment using structure from Motion photogrammetry in the laboratory

Gabriel Spreitzer[a,*], Jon Tunnicliffe[b], Heide Friedrich[a]

[a] Department of Civil & Environmental Engineering, University of Auckland, Auckland, New Zealand
[b] School of Environment, University of Auckland, Auckland, New Zealand

ARTICLE INFO

This manuscript was handled by Marco borga, Editor-in-Chief, with the assistance of Francesco Comiti, Associate Editor

Keywords:
Large wood (LW) accumulation models
SfM photogrammetry
Estimation of 2.5D and 3D volumes
LW accumulation porosity

ABSTRACT

A Structure from Motion (SfM) photogrammetry-based methodology for precise mapping of large wood (LW) accumulations in fluvial systems is presented. The technique may be useful for routine inventory and rapid volume estimation of complex LW structures that tend to divert or obstruct flow in rivers. Our methodology is validated by means of laboratory experiments, ranging from elementary to complex arrangements of LW components and organic fine material (OFM). Seven experimental setups were used as the basis for (i) manual approximations of 2.5D and 3D geometric reference volumes, (ii) 2.5D volume models based on mesh geometry, (iii) a closed ('watertight') 3D mesh from an unorganized point cloud and (iv) estimates of porosity. A commercially available SfM photogrammetry software package, Pix4Dmapper, was used for point cloud and simplified mesh generation. In order to obtain more precise volumes, 3D surface models are required. Accordingly, we generated 3D watertight mesh models of the unorganized point cloud using the screened Poisson Surface Reconstruction (PSR) technique. The Pix4D volume tool (2.5D) resulted in an overestimation (2.9 to 52.7%) of the geometric volume (3D), due to the convex hull approximation of the geometry normal to the surface plane. PSR (3D) resulted in more precise volumes, showing deviations from the geometric volume (3D) in a range of −15.9 to +10.6%, as the algorithm could capture concavities and involuted surfaces on the accumulation. Assuming that the difference between 3D and 2.5D volume models represents many of the voids visible within or on the surface of the deposit, this volume can be used as an estimate of porosity. Our assessment suggests that image-based SfM methodology is well-suited for further investigations in LW research, due to its time and cost efficiency in comparison with other conventional surveying techniques. The methodology can be used to generate high quality point cloud and mesh models of log jam formations; these may be used by river managers and researchers to quantify accumulation volume and thus gain a better understanding of LW composition and the influence of wood geometry on hydraulic flow conditions.

1. Introduction

1.1. Large wood (LW) accumulations and assessment

The majority of river-focused research defines large wood (LW) as wooden pieces with a minimum length of 1 m and a diameter larger than 0.1 m (Nakamura and Swanson, 1994; Fetherston et al., 1995; Wyżga and Zawiejska, 2005; Ravazzolo et al., 2015; Martin et al., 2018), while smaller elements are considered as organic fine material (OFM). LW plays an important role in moderating sediment transport and storage (Megahan and Nowlin, 1976; Hornbeck et al., 1993), and stream channel morphology (Zimmerman et al., 1967; Keller and Swanson, 1979; Bilby, 1984; Smith et al., 1993; Abbe and Montgomery, 1996), but it also provides habitat for fish and other riverine organisms (Fausch and Northcote, 1992). Several research projects have focused on the influence of log structures on channel forms, including stream banks and bars (Keller and Swanson, 1979; Gippel et al., 1996), as well as on flow hydraulics (energy losses, changes in roughness and flow dissipation) (Heede et al., 1972; Gregory et al., 1985; Knauss, 1995; Anderson et al., 2006). Besides the positive effects of wood in stream channels, LW accumulations at constricted cross-sections may represent a hazard to river-spanning infrastructure, agriculture lands, as well as human populations in adjacent areas (Mazzorana and Fuchs, 2010; Schmocker and Weitbrecht, 2013; Ruiz-Villanueva et al., 2017; Gasser et al., 2019).

A fundamental knowledge of geometrical arrangement, volume and porous space of LW accumulations is essential in order to better understand the effects on channel hydraulics in presence of log structures.

* Corresponding author.
E-mail addresses: gspr390@aucklanduni.ac.nz (G. Spreitzer), j.tunnicliffe@auckland.ac.nz (J. Tunnicliffe), h.friedrich@auckland.ac.nz (H. Friedrich).

https://doi.org/10.1016/j.jhydrol.2019.124430
Received 29 July 2019; Received in revised form 31 October 2019; Accepted 2 December 2019
Available online 05 December 2019

Furthermore, quantification of the wood inventory within a river corridor provides important information on the likelihood of jam development, as well as clues to key loading points within the contributing catchment. The geometry of LW accumulations is a function of the flows that deposited the wood (Wyżga and Zawiejska, 2005). Material deposited in the waning stages of a flood may be deposited individually or as bundles with similar orientation (Abbe and Montgomery, 2003). More often, an abrupt transition in flow conditions above a constricted passage will lead to a chaotic accumulation that can be several meters high (Lassettre and Kondolf, 2012; Rusyda, 2014), and several kilometres in length (Collins et al., 2002; Wohl, 2014). Interstitial space at the inside of the log formation can be filled by transported OFM, reducing accumulation porosity. Such LW accumulations can act as flow obstructions (Moos et al., 2018) that affect channel morphology (Mosley, 1981; Wohl and Scott, 2017). There is considerable scope for better capture and structural analysis of these jams, if the tools were available.

A current literature review reveals little progress in wood volume estimation techniques. Some studies have focused on assessing LW volumes along channels (Van Wagner, 1968; Uchiogi et al., 1996; Benda and Sias, 2003; Rigon et al., 2008), and only a small number have endeavoured to evaluate the volume of existing log jams. Those that focused on LW accumulation volume applied a parallelepiped approach (Boivin et al., 2015) or geometric measures of length and diameter as well as number of individual logs, or wood pieces (Cordova et al., 2006; Brown et al., 2014; Dixon and Sear, 2014; Ruiz-Villanueva et al., 2016; Tonon et al., 2018) and calculated a volume based on cylindrical approximations. These methods do not consider any irregularities in shape, and in many cases volume estimates are based on a line intersection technique introduced by Warren and Olsen (1964), leading to a rough estimation of LW volume rather than a precise measurement. Brown et al. (2014) also described the methodology of water displacement for LW volume estimation, which may be effective for relatively small quantities of organic material. Although "*measuring of volume is difficult*" (Harmon et al., 1986), many researches have underlined the importance of assessing LW volume within a quantitative assessment framework (Lienkaemper and Swanson, 1987; Gurnell et al., 2002; Webb and Erskine, 2003; Manners and Doyle, 2008; Dixon and Sear, 2014; Wohl et al., 2017; Martin et al., 2018).

Characterising the porosity of wood accumulations, in particular, still represents a major challenge in LW research (Piegay, 1993; Boivin and Buffin-Bélanger, 2010; Schalko et al., 2018; Scott et al., 2019), as it is onerous to estimate void space inside the log jam formation. Gaps in accumulations have important implications for hydraulic flow behaviour, such as the development of backwater effects, which are strongly related to the blocked cross-sectional area, the amount of OFM and accumulation porosity (Knauss, 1995; Schalko et al., 2016; Gschnitzer et al., 2017). Thus, improved assessment of void space within accumulations can help in evaluating structural integrity and capacity for retention of water and sediment.

Finally, any technique for rapidly acquiring consistent volume information will help to improve wood inventories and budgets of wood flux from catchments. Wood budgets are commonly used to study the impacts of forestry (Cave et al., 2017; Phillips et al., 2018) or other disturbances that affect wood supply to rivers. Drone photogrammetry is particularly helpful for this application, as the photographs can be taken from an aerial vantage, at a scale tailored for individual cases and at a resolution that is well-suited for reach studies (Colomina and Molina, 2014; Cunliffe et al., 2016; Woodget et al., 2017; Lucia et al., 2018). Higher altitude (e.g. airplane-based) photogrammetry (Smikrud and Prakash, 2006) does not provide sufficient detail for precise volumetric assessment.

Recent studies applied aerial (Sanhueza et al., 2019) and ground-based (Spreitzer et al., 2019) Structure from Motion (SfM) photogrammetry for volume estimation of larger wood quantities. However, both studies reported challenges with model resolution and a lack of standardised protocols. The aim of this paper is to demonstrate a Structure from Motion (SfM) photogrammetry-based workflow, considering a suite of meshing algorithms that can produce precise volumetric estimates for wood accumulations using point cloud resolutions in the order of many (10^2–10^5) points per square meter, such as achieved using TLS surveying (Boivin and Buffin-Bélanger, 2010; Tonon et al., 2014; Grigillo et al., 2015). This is the typical realm of models acquired from field photography (i.e. from ground level) (Mosbrucker et al., 2017; Verma and Bourke, 2019) or low-altitude drone acquisition (Woodget et al., 2017; Acuna and Sosa, 2019), which provides better time and cost efficiency (Westoby et al., 2012).

1.2. Structure from Motion (SfM) for LW research

SfM photogrammetry has proven to be a powerful technique for fieldwork, as one can produce highly detailed models with simply a camera and a few strategically placed orientation and scaling marks. Westoby et al. (2012) provide a useful summary of the field procedures, reconstruction algorithms and the SfM workflow. There are a number of software packages available for point cloud generation, both as open source - evaluated by Bianco et al. (2018) - as well as commercially licensed - evaluated by Alidoost and Arefi (2017). The effectiveness of SfM has been demonstrated for terrestrial mapping in the field (Javernick et al., 2014; Kraaijenbrink et al., 2016; Smith et al., 2016; Jugie et al., 2018; Li et al., 2018a; Tunnicliffe et al., 2018), and there are a number of studies that have successfully demonstrated the applicability of SfM in the laboratory (Chandler et al., 2000; Curran and Tan, 2010; Morgan et al., 2016; Wang et al., 2016; Balaguer-Puig et al., 2017; Seitz et al., 2018). The survey accuracy has been shown to be similar to other topographic measurement techniques, such as terrestrial or airborne LiDAR (Mancini et al., 2013; Kaiser et al., 2014; Ružić et al., 2014; Morgan et al., 2016; Filippelli et al., 2019), although SfM photogrammetry is generally more efficient considering costs and time (Peterson et al., 2015). The Trinity River Restoration Program (TRRP, 2018) provides some interesting comparisons of TLS and SfM point cloud models, where results reveal a higher point cloud density in the TLS models, whereas SfM provided a more detailed surface structure; multiple camera viewing angles resulted in more detailed relief on the wooden elements (Peterson et al., 2015), making this methodology more suitable for LW research. Surrounding water and non-static vegetation may affect the quality of SfM photogrammetry models because of feature distortion or the loss of tie points during the initial point cloud processing stage. Some of the studies have used standard smartphone cameras for data acquisition and concluded that results reveal point cloud quality equal to that of TLS (Wróżyński et al., 2017). Besides data acquisition, smartphones may also be of use for point cloud generation, processing and meshing, using the available hardware resources (Nocerino et al., 2017).

The technique of obtaining volumetric information from multi-view 2D images has been in practice for decades (Martin and Aggarwal, 1983), though the achievable resolution has soared with the advent of automated point-matching and new bundle adjustment techniques. Once a point cloud model of an object is generated, its volume can be computed either in 2.5D, on the basis of a plane with a predefined region bounded by the convex hull and an elevation grid, or in 3D, where no such restrictions apply. However, the elevation function becomes complex for unorganized point cloud models (Remondino, 2003), such as LW accumulation models. Currently, a common challenge is the identification and/or classification of landscape elements from detailed, yet often noisy point cloud data. LW research faces this problem as well, in particular for branches, rootwads and OFM, while wood logs have a generally cylindrical form, which presents a consistent geometric form for meshing and recognition algorithms. Raumonen et al. (2013) and Hackenberg et al. (2015) exploited the geometric architecture of trees and developed an approach for clustered point cloud reconstruction of trees using such cylindrical units.

Table 1
The number and dimensions of dowels as well as OFM used to assemble the miniature LW accumulations (Composition), the volume of each individual item (Partial Volume), and the total accumulation volume (Geometric Volume (3D)). Furthermore, an index of accumulation complexity is provided (Evolution Phase and Classification).

Accumulation	Composition (Piece × L × D)	Partial Volume ($\cdot 10^{-3}$ m^3)	Geometric Volume (3D) ($\cdot 10^{-3}$ m^3)	Evolution Phase Manners and Doyle (2008)	Classification Wallerstein et al. (1997)
One Dowel	1 × 300 mm × 46 mm	0.50	0.50	Phase I	Underflow / Dam Jam
Two Dowels	2 × 300 mm × 46 mm	0.50	1.00	Phase I-II	Underflow / Dam Jam
Six Dowels	6 × 400 mm × 32 mm	0.32	1.93	Phase I-II	Dam jam
Eight Dowels (high photo count)	2 × 300 mm × 46 mm	0.50	2.93	Phase II	Deflector / Bar Head Jam
	6 × 400 mm × 32 mm	0.32			
Eight Dowels (low photo count)	2 × 300 mm × 46 mm	0.50	2.93	Phase II	Deflector / Bar Head Jam
	6 × 400 mm × 32 mm	0.32			
OFM Accumulation	1 L OFM	1.00	1.00	Phase IV	Dam / Deflector Jam
Ten Dowels + OFM	1 × 200 × 10 mm	0.02	1.42	Phase III	Dam / Deflector / Bare Head Jam
	6 × 267 × 12 mm	0.03			
	1 × 200 × 18 mm	0.05			
	1 × 267 × 18 mm	0.07			
	1 × 267 × 22 mm	0.10			
	1 L OFM	1.00			

In this vein, recent work in related fields have shown successful reconstruction of individual plants with stem, branches and leaves, both on a basis of the most relevant neighbour points in SfM photogrammetry (Golbach et al., 2015), and TLS data (Hétroy-Wheeler et al., 2016). A significant advance in these studies was achieved by the clusterization of leaves and branches that allows for structural assessment and volume estimation (Schneider et al., 2014; Widlowski et al., 2014). Surface reconstruction for tubular shapes and tree sections is often based on the Poisson scheme (Morel et al., 2018), which has been shown to be robust and fairly stable in a number of studies (Kaiser et al., 2014; Carrivick et al., 2016; Gupta and Shukla, 2017). The accuracy of plant and tree reconstruction algorithms shows errors in a range of a few cm to less than one mm for an entire tree model (Hackenberg et al., 2015; Li et al., 2018b). LW research faces the additional challenge presented by complex compositional features, e.g. OFM and sediments, for which high point cloud density becomes essential in order to distinguish amongst some of these features (Colvard, 1998; Wright et al., 2000).

A recent study applying SfM photogrammetry to the problem of aboveground biomass estimation shows how compositional details can be captured based on a colour scheme (Alonzo et al., 2018). The method of colour segmentation algorithms for point cloud filtering has further been applied in geosciences for obtaining volumes and porosity of soil and sediments (Orru et al., 2016). When filtering a reconstructed surface model for colours, surface texture may be used for the generation of roughness models (Bertin et al., 2015; AlRatrout et al., 2018) and used for porosity estimates (Seitz et al., 2018). Approaches such as introduced by Raumonen et al. (2013) and Alonzo et al. (2018) can help to estimate LW accumulation structure and volume, even when significant portions of the logs are not captured in the dataset.

1.3. Objectives

Given the requirement for precise, in-situ volume estimation in LW research, there is high demand for portable and easily deployed surveying tools, such as SfM photogrammetry, that can efficiently capture the geometry of wooden deposits. To move from the unorganized point cloud produced by photogrammetric techniques to a volumetric model requires testing of the available meshing and volume integration algorithms, under controlled conditions. With our work we aim to develop a SfM photogrammetry-based workflow (pipeline) to estimate the volume of model LW accumulations that can be objectively verified.

Our objectives are:

(i) To generate high quality point cloud models of LW accumulations under controlled conditions in the laboratory,
(ii) To compute the geometric measures, including volume and porosity, of the generated 2.5D and 3D LW accumulation models,
(iii) To evaluate and assess the computed LW volumes generated via SfM photogrammetry in comparison with easily verifiable accumulation volumes,
(iv) To assess the challenges and opportunities arising from 2.5D volume estimation, from elevation points that have been projected vertically onto a reference surface, versus 3D volumes that may be obtained by detailed meshing of the point cloud.

SfM photogrammetry is a promising tool for LW research under controlled conditions in the laboratory, considering its performance relative to other available mapping techniques. Developing a quantitative framework for analysing LW accumulations will enable more meaningful and compatible measures of accumulation composition and volumes, as well as detailed assessment of surface structure, detrital organic characteristics and other features.

2. Laboratory experiments

For estimates of LW accumulation volumes, based on SfM photogrammetry, we used a set of wooden dowel structures, which were assembled on a smooth surface in the laboratory. The wooden dowels were of a uniform cylindrical shape, varying in length and diameter. Altogether seven distinctive accumulation structures (Table 1) were considered; starting with the most elementary – a single wood dowel – working up to complex LW accumulations. We also considered OFM as part of our experimental setup for a small number of experiments. For the laboratory OFM substrate we used wood chips with a length of up to 65 mm, and bark pieces in a range of 4–32 mm (b-axis). The OFM fills porous space in between the log skeleton structure, reducing accumulation porosity. The species of the wooden material was *Pinus radiata* (New Zealand Pine).

For the first experiment a single wooden dowel - One Dowel – with a length of 300 mm and 46 mm in diameter was used (Table 1). This setup appears trivial, however, it represents an essential verification test for further volume assessment of LW accumulations.

The second structure comprised two wooden dowels - Two Dowels – both showing equal dimensions (L = 300 mm, D = 46 mm). One of the dowels was placed on top of the other one, in a perpendicular alignment. The distance between the grounded point of the top dowel and the underlying, centrally-placed dowel was about three quarters of the top dowel's length.

Six cylindrical wooden dowels – Six Dowels (dowel pile) – were used for a further elementary LW accumulation. A triangular bundle was formed, with three logs at the base, two in the middle and one on

top. In order to maintain the shape and position of the dowel pile tape was used. The dowels had a length of 400 mm each, with a diameter of 32 mm.

A more complex LW accumulation was set up using eight wooden dowels - Eight Dowels (high photo count) - that were randomly assembled, forming an accumulation skeleton. The LW accumulation consisted of a mixture of the previously used dowels, comprising two dowels with a length of 300 mm and 46 mm in diameter and another six dowels with lengths of 400 mm and 32 mm in diameter. For this experiment a relatively high number of images (529) was obtained for the photogrammetric model.

Similar to the previous setup (Eight Dowels – high photo count), the same eight dowels were used and assembled into another LW accumulation - Eight Dowels (low photo count) - on the laboratory floor. A relatively low number of images (23) was acquired for the model. The purpose is to demonstrate the effects of having a low number of images in comparison to a high number of images for volume estimates.

An accumulation consisting of only OFM - OFM Accumulation - was formed to resemble a heap, approximately 70 mm in height with a roughly circular planform diameter of 190 mm. For material preparation, a measuring cylinder was filled with 1.00 10^{-3} m^3 of wood chips (< 65 mm) and bark pieces (4 to 32 mm). The glass cylinder was filled in three layers, with the material gently compacted at each interval, using fingers. The material in the measuring cylinder and in the accumulation heap showed a similar degree of consolidation.

The most complex LW accumulation considered for our experiments consisted of ten dowels, varying in length and diameter, and 1 L of OFM. The LW dowels were mixed up with the OFM and formed into a complex accumulation structure - Ten Dowels + OFM. Dowel composition and dimensions can be obtained from Table 1. The total 3D geometric volume based on the conical shape of the accumulation was $1.42{\cdot}10^{-3}$ m^3.

3. Methodology

3.1. Procedure for volumetric estimates

We classified our accumulations into three categories; (i) elementary accumulations (One Dowel, Two Dowels and Six Dowels), (ii) complex accumulations (Eight Dowels), and (iii) OFM accumulations as a further advanced stage of complex accumulations (OFM Accumulation and Ten Dowels + OFM). The aim of the experiments is to compare 3D and 2.5D volumes, estimated via SfM photogrammetry methodology, to the actual 3D (see 3D geometric volume in Table 1) and 2.5D volumes (see 2.5D geometric volume in Fig. 1), computed via standard mathematical approximations to resolve the geometric aspects of the constitutional elements (e.g., cylinders, cones, wedges).

The point cloud model was generated using a commercial SfM photogrammetry software package, Pix4Dmapper (Pix4D Switzerland, 2018) version 4.1.25, which provides an efficient workflow and offers a palette of useful tools for point cloud as well as mesh processing. The volumes of the 2.5D and 3D photogrammetrically-derived meshes were assessed using freely available, open-source software tools, namely, MeshLab (Cignoni et al., 2008) version 2016.12 and CloudCompareV2 (2016) version 2.6.3. In CloudCompare the initial unorganised point cloud model was segmented for further object-oriented processing stages, including filtering and cleaning of outlier points as well as meshing. The MeshLab implementation of the screened Poisson Surface Reconstruction (PSR) (Kazhdan and Hoppe, 2013) was used for meshing the unorganized point cloud, providing an initial mesh. The final refinement of the mesh involved closing the grid surface, such that it was continuous ('watertight'). For this operation we used the commercial package Autodesk Fusion 360 (2018) version 2.0.5119. Having established 2.5D and 3D volumes, the porous space inside the LW accumulations could be estimated as the volumetric difference between the two models.

3.2. Image acquisition

Experiments were mostly conducted in a custom-designed black room in the laboratory, consisting of black walls with good light conditions (4 × 500 W halogen flood lights) from the top and a table in the centre. A platform (400 × 500 mm) was mounted on the table, supporting a rotating platter with a flat surface. This platform enabled easy setup for obtaining oblique and nadir images without capturing any detail beyond the LW assembly (e.g. floor). The only experiment that was not conducted in the black room – Eight Dowels (low photo count) – was carried out on a sealed and flat laboratory floor. For scaling purposes, a number of chequerboards with a raster of 25 mm were placed around the accumulations.

Image acquisition for our LW volume assessment was carried out using a standard smartphone device – Huawei Nova 2i – with 16MP image resolution. Images were captured under controlled light conditions, using default settings for contrast, exposure, saturation and sharpness. Further camera specifications are listed in Table 2.

3.3. Point cloud and mesh processing in Pix4D

Pix4Dmapper initially computes matching key-points from overlapping images, then applies a bundle block adjustment algorithm to generate a sparse 3D point cloud (Step 1). Based on the residuals from model fitting, the software iteratively estimates the internal and

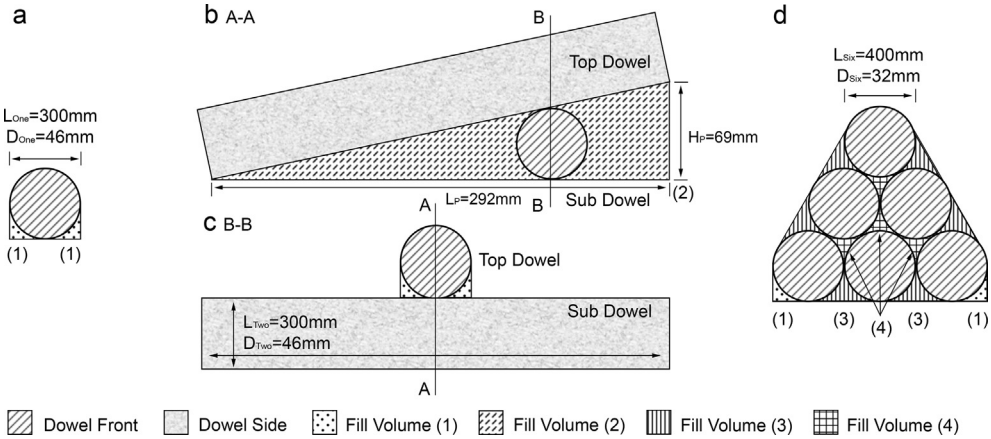

Fig. 1. Geometric Volume (2.5D): Geometric primitives for mathematical approximation of the 2.5D Volume for One Dowel (a), Two Dowels (b and c) and Six Dowels formed into a bundle (d). The fill volumes indicate the area according the applied mathematical equations.

Table 2
Camera specifications used for data collection in the laboratory.

	Huawei Nova 2i
Model	RNE-L22
MP	16 + 2 (secondary rear camera)
Format	JPEG image
Sensor type	CMOS BSI
Image Resolution (pixels)	4,608 × 3,456
Focal length (mm)	4.00
35 mm focal Length (mm)	27
ISO range	160 to 250
Exposure range (sec)	1/30 to 1/128
F-stop	2.2

external camera parameters until the best optimization is achieved (Pix4Dmapper, 2018). After initial sparse cloud processing, the model is scaled using ground control reference marks - in our case chequerboards around the LW accumulations. At this stage, the orientation of the point cloud model may also be adjusted by setting orientation constraints for the x, y and z directions. In order to take the new scaling and orientation input into account, the reprocessing step has to be started.

The next step in Pix4Dmapper involves computing the dense point cloud model and mesh (Step 2). The point cloud density settings are listed in Table 3, and the processing times required can be found in Table 4. A maximum number of $1.0{\cdot}10^6$ faces was selected for the generation of the Pix4D mesh model, which provides a good balance between acceptable model detail and tractable computation of volumes and other analyses. The third processing step (step 3) involves the generation of a digital surface model (DSM) and the orthomosaic; both are essential for volume estimates using the volume tool implemented in Pix4Dmapper (Pix4D Volume Tool 2.5D). The DSM is generated from nearest-neighbour interpolation of the dense point cloud; the orthomosaic provides detailed RGB information for the resultant DSM (Pix4Dmapper, 2018).

3.4. Geometric volume (2.5D)

Using an approach analogous to the 2.5D method in the Pix4D volume tool, we calculate the projected volume for elementary LW accumulations independently, using geometrical primitives. Based on the laboratory setup of the LW models for One -, Two - and Six Dowels, we assessed the volume of the primitives as well as the interstitial space between the objects and the horizontal reference plane (platter surface). The actual volume of a dowel is provided in Eq. (1); the fill volumes for various interstitial elements (1–4) are approximated using Eqs. (2)–(5).

For the first experimental setup, using one dowel, the projected volume was calculated as demonstrated in Fig. 1a using Eq. (6). The next accumulation model, comprising two dowels Fig. 1b and c, shows a projected length of 292 mm for the top dowel, emerging to a height of 69 mm (measured to the bottom edge of the top dowel). The total 2.5D volume is calculated according to Eq. (7). Another 2.5D calculation for the Six Dowel accumulation was assessed using Eq. (8). The dowel pile in Fig. 1d consists of several different void elements; calculations must account for the various projected volumes, including ledges and projections. Mathematical approximations in 2.5D resolution are only practical for elementary LW accumulations with known geometric measures; the method becomes inadequate as model complexity increases.

$$V_{\text{Dowel}} = \frac{D^2 \cdot \pi \cdot L}{4} \quad (m^3) \tag{1}$$

$$V_{\text{Fill Volume (1)}} = \frac{D^2}{4} - \frac{D^2 \cdot \pi \cdot L}{16} \quad (m^3) \tag{2}$$

$$V_{\text{Fill Volume (2)}} = \frac{L_P \cdot H_P \cdot D}{2} - \frac{D^3 \cdot \pi}{4} \quad (m^3) \tag{3}$$

$$V_{\text{Fill Volume (3)}} = \frac{D^2 \cdot \left(1 - \frac{1}{4} \cdot \pi\right)}{2} \quad (m^3) \tag{4}$$

$$V_{\text{Fill Volume (4)}} = \frac{D^2 \cdot (\sqrt{3} - \frac{\pi}{2})}{4} \quad (m^3) \tag{5}$$

$$V_{\text{One Dowel, Geometric Approximation}} = V_{\text{Dowel}} + 2 \cdot V_{\text{Fill Volume (1)}} \quad (m^3) \tag{6}$$

$$V_{\text{Two Dowels, Geometric Approximation}} = 2 \cdot V_{\text{Dowel}} + V_{\text{Fill Volume (1)}} + V_{\text{Fill Volume (2)}} \quad (m^3) \tag{7}$$

$$V_{\text{Six Dowels, Geometric Approximation}} = 6 \cdot V_{\text{Dowel}} + 2 \cdot V_{\text{Fill Volume (1)}} + 6 \cdot V_{\text{Fill Volume (3)}} + 4 \cdot V_{\text{Fill Volume (4)}} \quad (m^3) \tag{8}$$

3.5. Pix4D volume tool (2.5D) and PSR meshing (3D)

In the following work, we employ two techniques for 2.5D and 3D volume estimation. '2.5D' volume consists of a convex hull enclosing the horizontal extents of the point cloud, projected vertically from above, much as a sheet fully draped over an object encompasses the extent of the object and falls vertically to the floor. Thus, an elevation field (potentially including void space) can be mapped to a 2D raster grid and volume can be estimated by integrating the gridded height elements; this approach is commonly used in terrestrial and airborne surveys to generate volumetric information of, for instance, stockpiles or landforms above a given reference datum (Lane et al., 2003; Milan et al., 2007; Eltner et al., 2016). The 2.5D approach, however is not well-suited to subjects with over-arching structures, hollows, concavities or any surface whose face normals point below the plane of the horizontal reference surface (Spreitzer et al., 2019).

Pix4Dmapper was used to compute the 2.5D volume, which requires the specification of a base surface (Fig. 2). We selected multiple points on the flat surface around the LW accumulation and used the default settings for base surfaces. Points above (cut volume) and beneath (fill volume) the reference surface are kept in the computational domain, however they have separate outputs. In this article we are focusing on the cut volume. The base surface raster is resolved at the same

Table 3
Pix4D settings for processing of LW accumulations in the laboratory.

Process	Parameter	Setting
1.Initial Processing	Key Image Scale	Full
2.Point Cloud and Mesh	Point Cloud Densification -Point Density	Optimal
	Image Scale	Multiscale, 1/2 (Half image size, Default)
	Settings	Medium Resolution (8192x8192)
	Mesh Faces	$1.0{\cdot}10^6$
3.DSM, Orthomosaic and Index	Resolution	1 × GSD (1 mm/pixel)
	Filters	Noise: on ; Surface Smoothing: on – Type: Sharp
	Raster Generation	Method: Inverse Distance Weighting

Table 4
Point cloud and mesh specifications for the LW and OFM accumulation models.

Specifications	One Dowel	Two Dowels	Six Dowels	Eight Dowels (high photo count)	Eight Dowels (low photo count)	OFM Accumulation	Ten Dowels + OFM
Wood Dowels	1	2	6	8	8	0 (OFM)	10
Point Cloud							
Images total	77	139	215	529	23	130	263
Images calibrated	75	137	215	517	23	130	262
Images calibrated	97%	98%	100%	97%	100%	100%	99%
Camera optimization	99.99%	100%	99.99%	100%	99.85%	99.76%	99.94%
Number of 3D points	$2{,}89{\cdot}10^6$	$4{,}61{\cdot}10^6$	$5{,}82{\cdot}10^6$	$12{,}69{\cdot}10^6$	$2{,}22{\cdot}10^6$	$4{,}64{\cdot}10^6$	$6{,}78{\cdot}10^6$
Processing times							
1. Initial Processing	0.2 h	1.0 h	1.7 h	2.6 h	0.2 h	0.3 h	1.0 h
2. Point Cloud / Mesh	2.5 h	7.0 h	10.3 h	42.5 h	0.2 h	3.1 h	10.2 h
3. DSM / Orthomosaic	0.1 h	0.1 h	0.1 h	0.6 h	0.3 h	0.1 h	0.2 h
Acc. Mesh Models							
Number of faces Pix4D	$1.0{\cdot}10^6$						
Number of faces PSR	$3.3{\cdot}10^6$	$3.7{\cdot}10^6$	$2.6{\cdot}10^6$	$4.7{\cdot}10^6$	$3.3{\cdot}10^6$	$10.8{\cdot}10^6$	$15.2{\cdot}10^6$
PSR Box Dimensions							
x (m)	0. 319	0.309	0.403	0.562	0.673	0.217	0.423
y (m)	0.099	0.309	0.107	0.424	0.474	0.212	0.287
z (m)	0.057	0.115	0. 127	0.192	0.156	0.084	0.128
PSR Mesh Density (faces·cm^{-3})	1,833	337	484	103	66	2,795	978

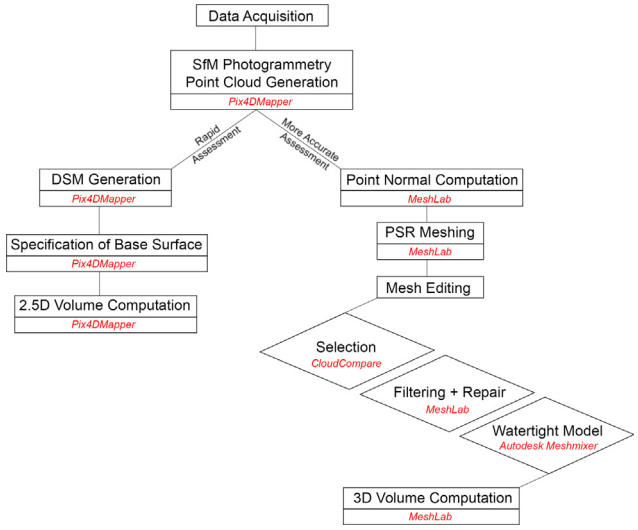

Fig. 2. Graphical illustration of the workflow for obtaining the 2.5D Pix4D and 3D PSR Volume.

resolution as the model ground sampling distance (GSD).

In contrast to the 2.5D approach, the 3D model mesh encloses the object from all perspectives, and volumes are assessed by integrating cubes or tetrahedral elements within this enclosed space (Wang et al., 2018). This is the preferred technique in the present application, since the aim is assessing the volume of wooden material within a complex body with many voids. With photogrammetric techniques, the field of view into the LW accumulations is invariably obscured by interwoven wooden elements, OFM and sedimentary fill, so our assessment of deposit porosity is imperfect even with 3D models, but we think this is an important improvement over more conventional 2.5 techniques.

The generation of robust 3D meshes of LW accumulation bodies using PSR was conducted in MeshLab, CloudCompare, and Autodesk Fusion 360. The variety of software packages applied in our workflow (Fig. 2), is a function of the many tasks involved in the reconstruction of LW accumulations; each program features specialized tools for mesh creation, editing (filtering and cleanup) and construction of a watertight hull. As a first step, after importing the point cloud model, the computation of point normals is required (Mitra and Nguyen, 2003). This was done using orientation consensus among 12 neighbour points, with view direction from the top, as this arrangement generally resulted in the most satisfactory surface reconstruction, with minimal artefacts. For PSR an octree depth of 12 was chosen, and other parameters were kept as default. Once the PSR meshing was finished, the resultant grid was exported to CloudCompare in order to isolate the area of interest – the accumulation structure – from the surrounding platter topography. CloudCompare was found to have the best tool for this operation.

Back in MeshLab several filter and reconstruction processes were applied; (i) selection of edges longer than some optimum threshold ($5{\cdot}10^{-3} \pm 2.5{\cdot}10^{-4}$) (varies between the mesh models), (ii) selection of faces by colour (filtering for else than brown colours), (iii) filter for isolated faces with a diameter larger than some optimum (5–20% of the world unit) (varies between the mesh models), (iv) close holes (closing of resulting smaller holes, not resolving the problem of closing the bottom of the mesh), (v) remove non-manifold edges/faces and zero area faces. The cleaned PSR mesh model is then exported in OBJ format for further processing in Autodesk Fusion 360. Autodesk Fusion 360 has tools for closing the bottom of the mesh with a smooth curved surface (rather than a plane or bulging protrusion, as often occurs in other methods) for the final watertight accumulation model. In some cases other parts of the PSR mesh– especially small sections on the bottom plane – become isolated while closing the hole. For this reason we filtered the mesh model once more in MeshLab and computed geometric measures. The output metrics provide information about bounding box dimensions, surface area and volumetric measures of the modelled LW accumulation.

3.6. Porosity of LW accumulations

In the present article void volume (V_v) is defined as the difference between the projected 2.5D volume ($V_{2.5D}$) and the more refined 3D volume (V_{3D}) (Eq. (9)). Consequently, the porosity (n) can be determined as the ratio of porous space (V_v) to 2.5D volume (Eq. (10)). For the OFM accumulations, the corresponding reference volume (3D geometric volume in Table 1) includes pore space.

$$V_v = V_{2.5D} - V_{3D} \quad (m^3) \tag{9}$$

$$n = 100 \cdot \frac{V_v}{V_{2.5D}} \quad (\%) \tag{10}$$

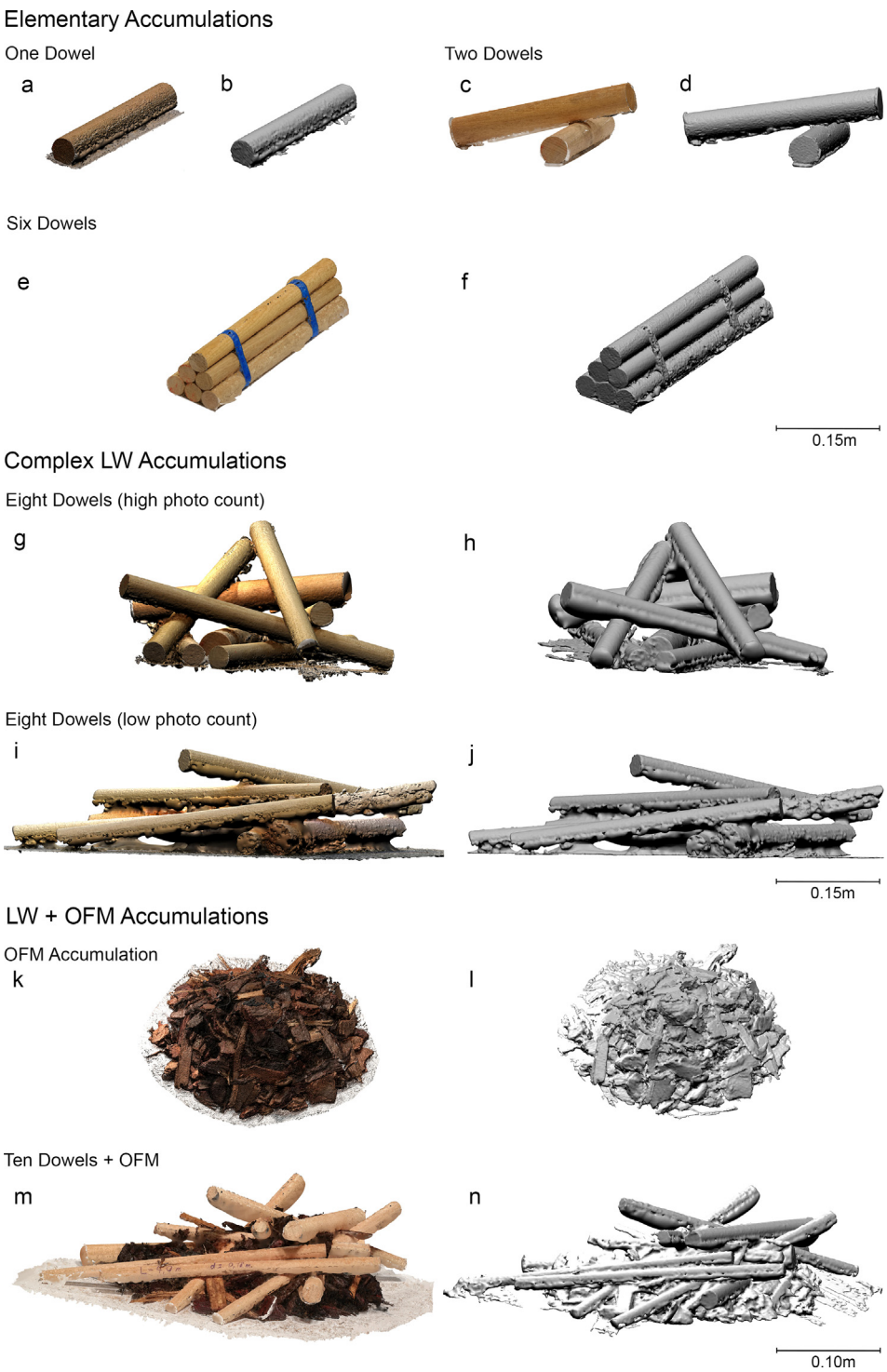

Fig. 3. 3D models of our miniature LW accumulations. Elementary accumulations are shown from a to f, more complex accumulation structures (g to j) and a mixture of wood dowels and organic fine material (OFM) (k to n). Mesh generated via PSR (left), and the fully closed 3D body of the corresponding LW accumulation (right).

4. Results

4.1. Point cloud and mesh results

All of our laboratory LW accumulations resulted in high-resolution point cloud models, with $2.2{\cdot}10^6$–$12.7\ 10^6$ generated 3D points. The processing time in Pix4Dmapper for initial tie point processing was between 10 min, for low image datasets, and 2.6 h for datasets with a higher number of images. Further point cloud processing times, including DSM and orthomosaic generation, ranged from 30 min to 43 h. Our 2.5D volume models, computed and meshed in Pix4Dmapper, emerged with $1.0{\cdot}10^6$ faces, as per description in the methodology (Section 3.3).

The 3D PSR algorithm generated between $2.6{\cdot}10^6$ and $15.2{\cdot}10^6$ faces, depending on the dowel prototype complexity. Meshing the Eight Dowels (low image) point cloud required two applications of the meshing process, in order to construct a watertight surface.

Table 4 provides an overview of point cloud and meshing results. Using PSR, the volumes of elementary LW accumulations were computed (Fig. 3a to f). The PSR operation, for the elementary LW

Table 5
Estimated volume and porosity values for LW accumulation models in the laboratory.

	One Dowel	Two Dowels	Six Dowels	Eight Dowels (high photo count)	Eight Dowels (low photo count)	OFM Accumulation	Ten Dowels + OFM
Volume							
Geometric Volume 3D (m^3)	$0.50{\cdot}10^{-3}$	$1.00{\cdot}10^{-3}$	$1.93{\cdot}10^{-3}$	$2.93{\cdot}10^{-3}$	$2.93{\cdot}10^{-3}$	$1.00{\cdot}10^{-3}$	$1.42{\cdot}10^{-3}$
Geometric Volume 2.5D (m^3)	$0{,}56{\cdot}10^{-3}$	$1{,}45{\cdot}10^{-3}$	$2.31{\cdot}10^{-3}$	–	–	–	–
Pix4D Volume Tool 2.5D (m^3)	$0{,}56{\cdot}10^{-3}$	$1{,}46{\cdot}10^{-3}$	$2{,}31{\cdot}10^{-3}$	$6{,}19{\cdot}10^{-3}$	$5{,}66{\cdot}10^{-3}$	$1{,}03{\cdot}10^{-3}$	$2{,}16{\cdot}10^{-3}$
PSR Volume 3D (m^3)	$0.49{\cdot}10^{-3}$	$0.98{\cdot}10^{-3}$	$2.13{\cdot}10^{-3}$	$2.95{\cdot}10^{-3}$	$3.27{\cdot}10^{-3}$	$0.86{\cdot}10^{-3}$	$1.46{\cdot}10^{-3}$
Porosity							
Porous Space (m^3)	$0.07{\cdot}10^{-3}$	$0.49{\cdot}10^{-3}$	$0.18{\cdot}10^{-3}$	$3.24{\cdot}10^{-3}$	$2.38{\cdot}10^{-3}$	$0.17{\cdot}10^{-3}$	$0.70{\cdot}10^{-3}$
n (%)	12.8	33.1	7.7	52.3	44.1	16.1	32.2

accumulations (2.6–3.7·10^6 faces), only takes a few minutes in MeshLab. Processing times increase slightly with more complex laboratory models (e.g. with OFM, 10.8 and 15.2·10^6 faces), however, the maximum time required for PSR was one hour for the Eight Dowels (high photo count) accumulation model, showing a total of 4.7·10^6 faces. The final meshes are shown in Fig. 3a ton, with the PSR model on the left side and the corresponding watertight model on the right side.

4.2. Volumetric results

Results for (i) 3D geometric volume, (ii) 2.5D geometric volume, (iii) Pix4D volume tool volume (2.5D), and (iv) PSR volume (3D) are outlined in Table 5 and summarised as a chart in Fig. 5. A selection of the Pix4D mesh models is shown in Fig. 4, with base surface in green and computed 2.5D volume in red. The 3D geometric volumes ranged from 0.50 up to $2.93{\cdot}10^{-3}$ m^3, while computed 2.5D Pix4D volumes ranged between 0.56 and $6.19{\cdot}10^{-3}$ m^3. In contrast, the 3D PSR volumes, displayed in Fig. 3 at the left-hand side, ranged from 0.49 to $3.27{\cdot}10^{-3}$ m^3. Some individual OFM pieces are resolved, emphasising the high level of mesh detail. The 3D PSR models reveal pore space volumes that are almost identical to the 3D geometric estimates. As shown in Fig. 3 surface texture is reconstructed using screened PSR. Accumulation shape and size are kept intact when closing the bottom hole (Fig. 3 right side models).

For the first experimental setup using one dowel, the results displayed in Fig. 5 showed a discrepancy (surplus) of 10.9% between the volume computed via Pix4D volume tool (2.5D) and the 3D geometric volume. On the other hand, results from the Pix4D volume tool showed a minor underestimation (1.2%) relative to the 2.5D geometric volume approximation. Within the 3D framework, the PSR revealed a slight underestimation of volume in comparison to estimates based on 3D geometry. The pore space under the longitudinal edges of the dowel ('Fill Volume 1' in Fig. 1) was calculated to be 12.8%, according Eqs. (9) and (10).

Results for our second LW accumulation, comprising two identical wooden dowels, showed an overestimation by 31.9% in 2.5D volume, computed via algorithms in the Pix4D volume tool, compared to the 3D geometric volume. As before, almost identical values were achieved for 3D volumes (PSR vs 3D geometric volume), and 2.5D volumes (Pix4D vs 2.5D geometric volume). For this experiment a porosity of almost one third of the entire LW accumulation was calculated.

The dowel pile, consisting of six identical wooden dowels, showed considerable deviations amongst the 2.5D Pix4D volume tool ($2.31{\cdot}10^{-3}$ m^3), 3D PSR ($2.13{\cdot}10^{-3}$ m^3) and geometric volumes ($2.31{\cdot}10^{-3}$ m^3 (2.5D); $1.93{\cdot}10^{-3}$ m^3 (3D)). Variations of +9.5% for PSR volume and 16.4% for Pix4D volume tool were determined in comparison to the 3D geometric volume. Again, the 2.5D Pix4D volume tool and 2.5D geometric volume approximation showed almost

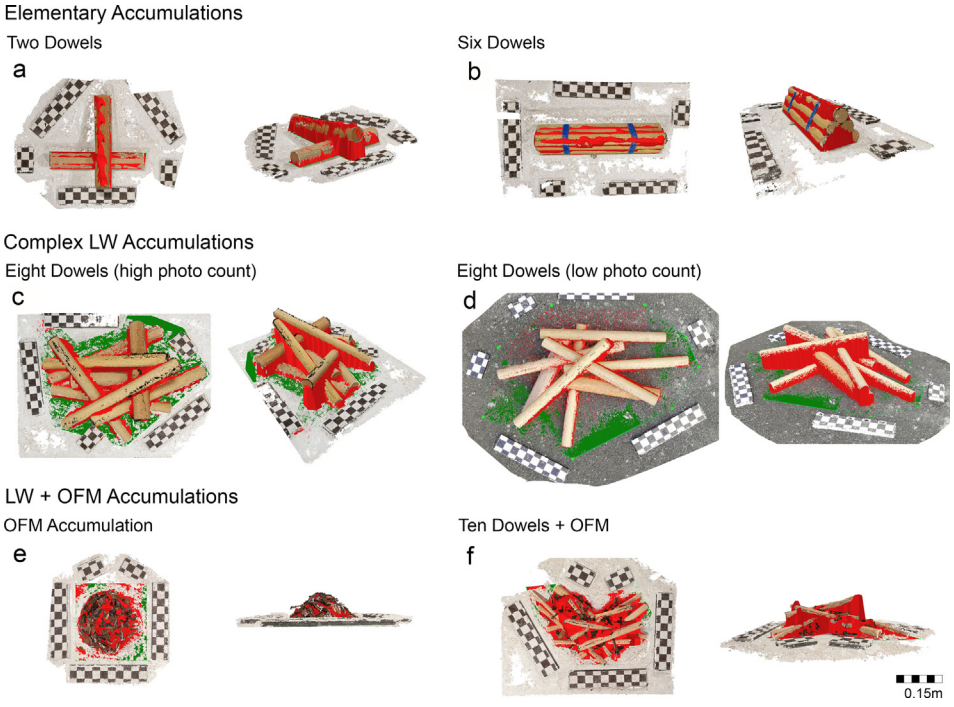

Fig. 4. Volume estimates from Pix4D volume tool (2.5D). The base surface is shown in green, and the modelled volume is displayed in red. The chequerboards (raster of 25 mm) are used for point cloud and model scaling. (For interpretation of the references to colour in this figure legend, the reader is referred to the web version of this article.)

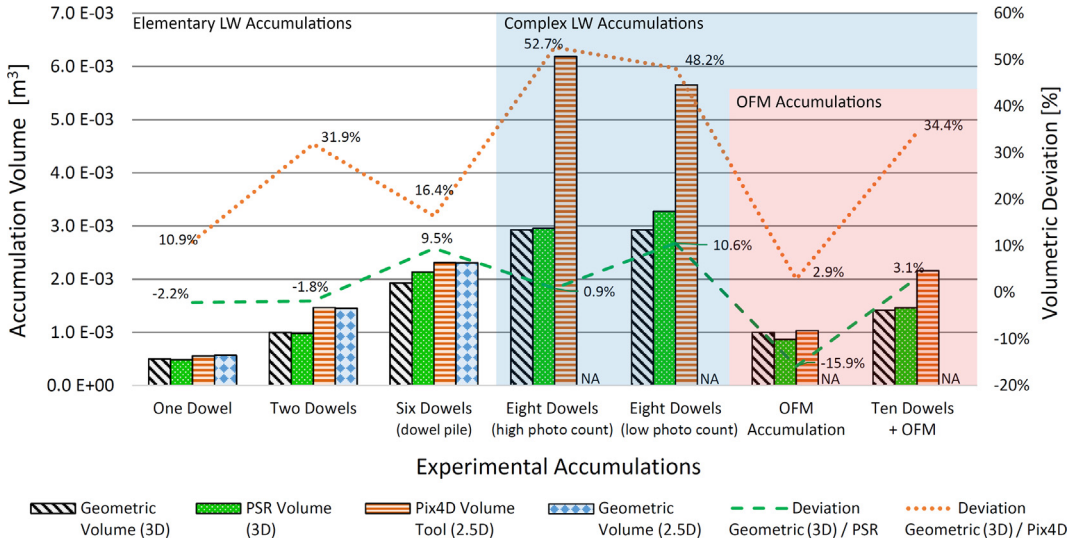

Fig. 5. Volumetric results for elementary and complex LW accumulations, considering the geometric volumes obtained in 2.5D and 3D, as well as volumes assessed using Pix4D volume tool (2.5D) and PSR.

identical measures (+0.2%). The volume of porous space in the dowel pile was calculated to be 0.18 L (7.7%).

More complex LW accumulations consisting of eight dowels, scanned with a high photo count (529 images), revealed nearly identical results between 3D PSR volume ($2.95{\cdot}10^{-3}$ m^3) and 3D geometric volume ($2.93{\cdot}10^{-3}$ m^3). The volume obtained using the 2.5D Pix4D volume tool ($6.19{\cdot}10^{-3}$ m^3), however showed a 52.7% deviation from those 3D volumes. This LW accumulation was not amenable to geometric volume calculation, owing to its complexity. The large deviation between 2.5D and 3D volumetric measures was attributed to a porosity of 52.3%.

The second LW accumulation also comprised eight dowels, however the point cloud and mesh were generated from a small image set (23 images); this model showed larger deviations between 3D PSR volume ($3.27{\cdot}10^{-3}$ m^3) and 3D geometric volume ($2.93{\cdot}10^{-3}$ m^3). Yet the value estimated via the Pix4D volume tool ($5.66{\cdot}10^{-3}$ m^3) indicated a slightly lower deviation for the 2.5D volume, consistent with the estimated porosity (48.2%). The magnitude of these departures is compared in Fig. 5.

Experiments with the OFM accumulation yielded almost identical values between 2.5D Pix4D volume estimates ($1.03{\cdot}10^{-3}$ m^3) and those obtained from 3D geometric volume ($1.00{\cdot}10^{-3}$ m^3) estimates. 3D PSR volume ($0.86{\cdot}10^{-3}$ m^3), however, revealed a negative departure of 15.9% from these volumes. In combination with ten LW pieces the 3D PSR volume ($1.46{\cdot}10^{-3}$ m^3) overestimated the 3D geometric volume ($1.42{\cdot}10^{-3}$ m^3) by 3.1%, whereas the 2.5D volume computed with Pix4D volume tool ($2.16{\cdot}10^{-3}$ m^3) exceeded this by 34.4%. The resulting porosity accounted for almost one third of the 2.5D volume (32.2%).

5. Discussion

5.1. Processing of elementary and complex LW accumulations in the laboratory

Despite the variable number of images, exclusively obtained from a standard smartphone camera with default settings, for each of the accumulation models, all of the point cloud models showed a high level of detail; this is most evident in the more complex models where sticks and bark are finely resolved. The model point cloud complexity varies considerably, so does the quantity of generated 3D points. As results have shown, the total number of model points relates directly to the number of photos used for the model generation (cf. Fig. 6). This was found to be consistent with existing literature applying ground-based SfM photogrammetry in geosciences (Stumpf et al., 2015; Wróżyński et al., 2017). Furthermore, it has been shown that with a larger degree of image overlap the number of generated points increases (Morgan et al., 2016). More complex LW accumulation models thus require a proportionately higher number of images with generous image overlap (> 75%), to resolve intersections of structural members, overlapping and covered areas, as well as void spaces inside the structure. An increased number of images and higher point density can counteract problems such as outliers, noise, perspective deformations, and poor reconstruction of sharp edges or similarly textured sections (Scaioni et al., 2015). These issues may be particularly acute for model subjects with pronounced surface irregularities, higher proportions of OFM and variable particle size (Li et al., 2018a).

We found that in terms of surface reconstruction (PSR meshing), models with OFM have up to four times more computed faces than LW accumulation skeletons, even with a similar number of images. This is evident when comparing results for Six Dowels and OFM Accumulation: despite a slightly lesser number of photos used to build the model, the OFM Accumulation has far more faces in the resulting mesh. From this we infer that face count must be strongly related to textural complexity of the surface. Higher image complexity likely provides more point-matching opportunities for the software, resulting in a denser overall point cloud (Maiti and Chakravarty, 2016). In contrast, less feature-rich subjects (e.g. One Dowel) will tend to have simpler resultant models, as the PSR algorithm smooths out noise associated effects (Kazhdan et al., 2006).

If a ceiling is set for the total face count ($1.0{\cdot}10^6$ faces, in our case), Pix4Dmapper may not be able to satisfy conditions for a clean mesh within that limit. The resulting, relatively coarse mesh surface structure, may therefore influence volumetric measures of LW accumulations, showing complex surfaces with only loosely resolved elements (Giirsoy and Patrikalakis, 1992; Shao et al., 2018), such as protruding branches, root wad, and entire logs. For one of our PSR mesh models, Eight Dowels (low photo count), a watertight surface could not be achieved initially due to this limit on vertices, and a number of artefacts such as self-intersecting faces were evident. We resolved this issue by re-meshing the existing PSR mesh with the same initial parameters and settings as were applied in the first instance for PSR in MeshLab, in order to achieve a watertight surface covering the entire LW accumulation. The resulting accumulation model (Fig. 3h) shows less detail than the model that was generated on the basis of a very high photo count (Fig. 3j).

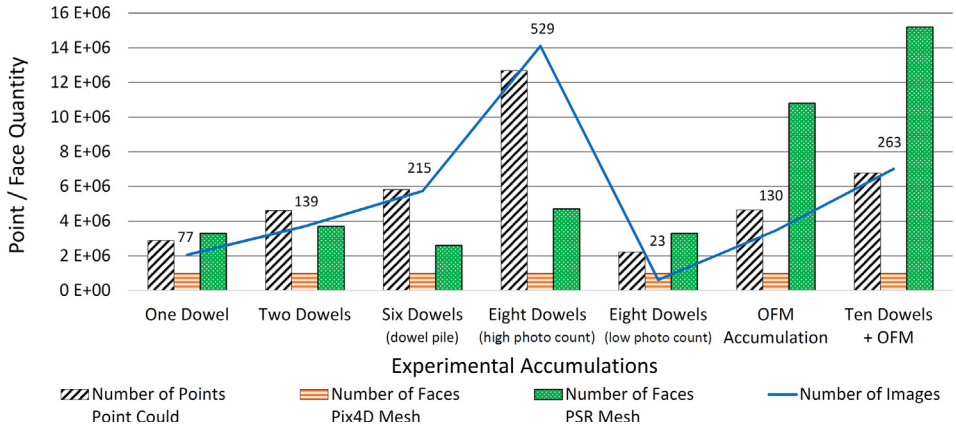

Fig. 6. Number of 3D points and faces used for constructing the LW accumulation models.

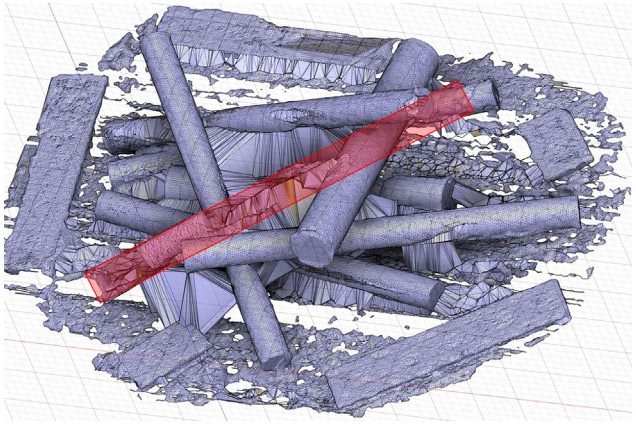

Fig. 7. Closing the bottom hole failed due to incorrect point normal computations, as an example for the Eight Dowels (high photo count) LW accumulation. The position of a missing dowel (not reconstructed in the PSR model) is delineated in red. (For interpretation of the references to colour in this figure legend, the reader is referred to the web version of this article.)

Results also reveal that processing times are proportional to the number of 3D points used for densified point cloud generation (Table 4). However, we also found that the relatively long processing times, which are required for densified point cloud generation using a high photo count, resulted in better model reconstruction than those generated on a basis of a low photo count. This means that there are compromises to be made between processing times, model accuracy and field labour in the course of image acquisition. The software algorithm requires relatively little operator intervention and can be scripted, to generate a great number of high resolution, densified point cloud models. With available options of subsampling and subdividing the point cloud, in order to better manage large data sets (Zhou and Chen, 2011; Fan and Atkinson, 2019), the remaining editing and mesh processing times can be reduced significantly, while maintaining surface details and mesh model quality (Tazir et al., 2016; Chen et al., 2017). The exact effects of subsampling and meshing of reduced LW accumulations point cloud models, however require further research to be better understood.

5.2. Point normals

The orientation of point normals is particularly important for elementary accumulations, given that there are fewer and larger faces available to represent the model topology. Reconstructing the contours of occluded and obscured elements is a troublesome problem in computational geometry (Hoppe et al., 1992; Mitra and Nguyen, 2003; Demarsin et al., 2007), as other results from the PSR process highlight (Fuhrmann and Goesele, 2011; Lobos and Rojas-Moraleda, 2013; Wolff et al., 2016; Sheng et al., 2018). As can be seen in Fig. 3h, i and j, a convex hull is generated at the bottom (occluded) side of individual LW pieces, which is a common effect when working with PSR, due to the inconsistent off-surface constraints (Mostegel and Rumpler, 2012; Berger et al., 2017; Guerrero et al., 2018). Ideally, all of the surface normals of each dowel would be neatly directed outward from the central axis. Fixing this problem is very time- and memory-consuming, and prone to producing unreliable data and failed convergence of mesh generation routines. The parameters contributing to the challenge are various (Vosselman et al., 2004), such as orientation of the cylinder axis or the detection of a circle in a plane (Kimme et al., 1975), describing the accumulation of randomly assorted cylindrical objects. This is an indication of present challenges when it comes to point cloud and meshing algorithms (Nurunnabi et al., 2017). The meshing software typically makes some bulk assumptions about normal direction (e.g. averaging amongst neighbouring normals, smooth iterations, or flip normal with respect to upward-pointing geometry or radial expansion starting from the centre) (Cignoni et al., 2008; CloudCompareV2, 2016), which, in the case of complex scenes, still can result in complete failure of point normal estimation and the process of generating a watertight mesh. In the case of a large number of point normals facing incorrectly, the entire dowel may not be considered for surface reconstruction (volume estimates), rather, it will get lost as a consequence of errors during the mesh closing procedure (Fig. 7).

It is desirable that the numerous details of LW accumulations, in shape and structure, be kept throughout each processing step in order to not affect volumetric assessment and calculation of accumulation porosity. Difficulties arising with unorganised point clouds and imperfections in point normal estimation and surface reconstruction need to be addressed. Future algorithms have to be robust to unoriented point normals and inaccuracies (Berger et al., 2014). We overcame meshing challenges by experimenting with the number of neighbours (up to 300 points) for complex LW accumulations, which resulted in a suitable, however not perfect, point normal computation for surface reconstruction and volume computation.

5.3. Volumetric computations

We have demonstrated that 2.5D computations using the Pix4D volume tool perform as expected – the models are consistent with our geometric estimations of the 2.5D models, all within a range of ± 1.2% volume deviation (Table 5). Overall, the 2.5D model from photogrammetry, such as also applied in the field (Spreitzer et al., 2019), is more convenient to develop than a watertight 3D mesh, which requires several software packages, as well as advanced skills in point cloud and mesh editing. Thus, from the perspective of rapid assessment of LW

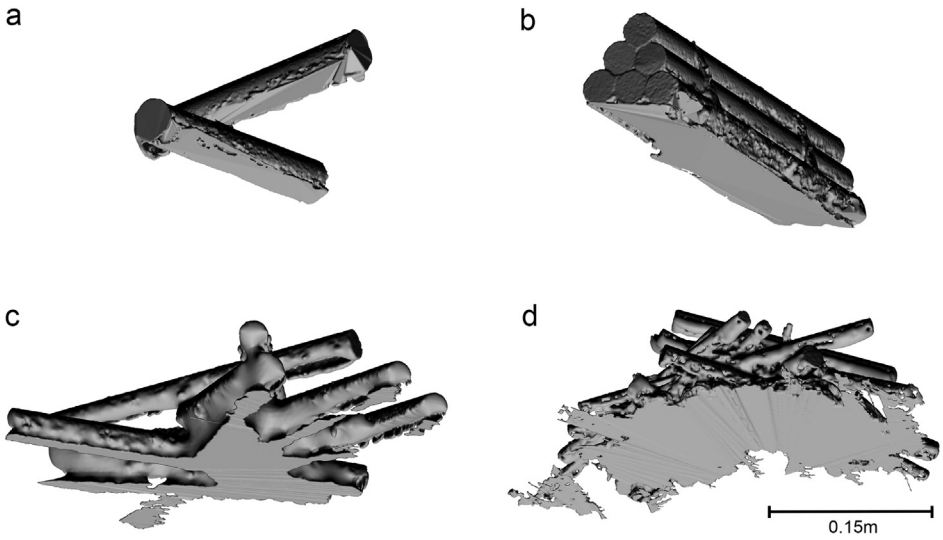

Fig. 8. Reconstructed watertight 3D PSR mesh models of our miniature LW accumulations. For Two Dowels (a), Six Dowels formed into a pile (b), Eight Dowels (low photo count) (c) and Ten Dowels + OFM (d).

volume, it may be reasonable to accept errors inherent in this approximation, and quantify 2.5D volume by using a standalone SfM photogrammetry software kit, such as Pix4Dmapper. Yet, there is a variety of SfM photogrammetry toolboxes available, freely (Astre, 2015; VisualSFM, 2018) or commercially, such as Agisoft LLC Russia (2018) and Autodesk ReCap (2019).

If more precision is needed, particularly when dealing with significant deposit complexity showing overarching structures, void spaces and protruding elements, it may be worth the additional effort to develop a fully 3D-resolved model, such as suggested in this study. In our experience, the PSR meshing algorithm followed by a mesh closing procedure provided the best surface reconstruction and volume estimates, as has also been demonstrated in the course of previously conducted studies (Kaiser et al., 2014; Carrivick et al., 2016; Gupta and Shukla, 2017). Considering the employment of the presented 3D SfM photogrammetry approach for field applications, special attention must be paid at a stage of closing the bottom of the mesh, which requires a basal surface that matches field conditions with a similar shape such as applied for the 2.5D Pix4D approach.

Relative to the 3D geometric models, the 3D PSR volumes are overestimated by a maximum of 10.6% for elementary and complex LW accumulations, all showing accumulation skeletons. In the case of large amounts of OFM filling some of the void spaces inside the accumulation skeletons, as demonstrated with experiments using OFM accumulations in Fig. 3k to n, negative discrepancies of up to 15.9% were found (3D PSR mesh resulted in lower values). This underestimation is likely related to the complex surface structure of the organic material. The digital mesh surface conforms more closely to the fibrous mass than could be captured during measurement using a glass measurement cylinder, when 1 L of OFM was prepared (c.f. OFM Accumulation and Ten Dowels + OFM in Section 2). While void spaces between glass cylinder wall and the OFM have been accounted for in the 3D geometric model, the 3D PSR mesh analysis did not capture such 'boundary void spaces', resulting in the slight negative aberration from the reference volume.

Another important factor is the number of images used for the photogrammetric model: a higher photo count typically resulted in greater detail and accuracy (Dikovski et al., 2014; Micheletti et al., 2015). The models that were based on a lower photo count led to blocky reconstruction and less refined joints between dowels. Furthermore, with a lack of oblique imagery, the meshing process fails at the reconstruction of occluded areas in the model (Mosbrucker et al., 2017). In places where multiple dowels intersect and overlap, PSR (usually very robust to noise (Wolff et al., 2016)) struggles with the identification of individual dowels. There are problems with filtering residual noise from point cloud generation (Williams et al., 2018), and the algorithm fails to accurately reconstruct dowel intersections. These circumstances provide reason to expect significant distortions in 3D volume, for models developed from a low photo count, because of sparse or over-inflated (due to the generation of a randomly shaped artefacts) reconstruction in the centre of the dowel accumulation.

In the case of Eight Dowels (low photo count) the 3D PSR mesh volume exceeded the 3D geometric volume by 10.6% (compare Fig. 5), whereas the PSR volume considering the Eight Dowels (high photo count) accumulation model revealed 0.9% volumetric difference, relative to the 3D geometric model. This scenario addresses once more the importance of obtaining a high-quality dataset, consisting of an abundant number of images, both oblique and nadir oriented, but also providing sufficient image overlap, both vertically and horizontally around the LW accumulation, as previous studies have confirmed (Dikovski et al., 2014; Micheletti et al., 2015). In order to provide optimum definition of compositional details and surface structure of the LW accumulation, we strongly recommend acquisition of additional images of the accumulation, with attention to voids and ledges, to better resolve contact points of major structural items.

Finally, closure of the mesh bottom can result in distorted surface reconstruction if the edges of the LW accumulation mesh model are not properly cleaned, as described in Section 3.5. The closed bottom surfaces of some LW accumulation models are shown in Fig. 8. Convex artefacts (bubbles) are generated when outlying mesh elements are encountered below the LW accumulation model. Ideally the resultant bottom surface is flat and shows sharp edges connecting to the existing LW accumulation model, as demonstrated in Fig. 8, rather than bulged corners that distort the actual accumulation volume. Cleaning the mesh model is therefore essential and enables the computation of realistic LW volumes from the 3D models.

Achieving a closed mesh is essential for 3D volume estimations, and we have yet to find a satisfactory open-source software solution for this operation. Alternatively, we were able to accomplish this rapidly, with few artefacts, in Autodesk Fusion 360.

5.4. LW accumulation porosity

LW accumulation porosity (n) is defined as the ratio of void volume to bulk volume (Pagliara and Carnacina, 2010). For porosity estimates of our LW accumulation models in the laboratory, we applied the 2.5D volume results from the Pix4D volume tool as the bulk volume, and the

3D PSR volume as solid volume, according to Eqs. (9) and (10). Results for accumulation porosity vary in a range of 7.7–52.3% (Table 5). The accuracy of this technique is limited by the scale of investigation; with larger accumulations, it becomes increasingly difficult to capture interior interstices and evaluate an aspect ratio (e.g. length, diameter) as well as the packing matrix of structural elements and OFM. However, it provides a good approximation and would be useful for first-order assessment of porosity characteristics across a population of LW deposits, both in the field as well as in the laboratory. Our porosity estimation approach has great potential for field applications and the improvement of recent SfM photogrammetry studies (Sanhueza et al., 2019; Spreitzer et al., 2019), as there are no visual estimates or manual calculations involved (such as a parallelepiped approach (Boivin et al., 2015; Livers et al., 2015; Scott et al., 2019), and the introduced 3D approach is a major advance for the development of semi-automated and automated methods, which allow for accurate LW accumulation volume and porosity assessment. The porosity results correspond to expected values, ranging from 30 to 50% (Dixon, 2016).

Additional information provided by SfM photogrammetry; e.g., colour information (Orru et al., 2016), can significantly contribute to resolving accumulation structure and jam porosity. The CANUPO plugin in CloudCompareV2 (2016) can be leveraged for automated identification and classification of point values, which works similar to classifiers for land cover mapping (Waske and Braun, 2009; Rodriguez-Galiano et al., 2012), and objects within a scene (Yousefhussien et al., 2018). Furthermore, previously developed reconstruction algorithms of tree and plant parts (Raumonen et al., 2013; Hackenberg et al., 2015), may be particularly helpful for skeletonisation of LW accumulations, based on progressive simplification of the geometry of structural members (Yrttimaa et al., 2019). Jacobson et al. (2013) developed a robust method, which uses surface texture to reconstruct a tree skeleton. This will be of major importance for future applications dealing with aspect ratios (packing matrix) (Zhang et al., 2006), roughness parameters (e.g. sediment and flow retention) (Bocchiola et al., 2002; Pagliara and Carnacina, 2010), obtained via SfM photogrammetry (Bretar et al., 2013; Verma and Bourke, 2019). This paths the way for using LW accumulations, showing most realistic features, in computer aided 2D (Ruiz-Villanueva et al., 2014; Costabile and Macchione, 2015; Ventres-Pake et al., 2019) and 3D (Smith et al., 2011; Allen and Smith, 2012; Lai, 2016) modelling.

6. Conclusions and outlook

Here we have demonstrated that both detailed '2.5D' volume surfaces and '3D' volumetric meshes can be generated in order to assess the volume of a scaled LW accumulation in a laboratory setting. As drone- or ground-based photogrammetric techniques are becoming increasingly popular to quantify and model LW formations in river systems, it is important to understand the potential and limitations of the technology. While SfM photogrammetry on small and accessible wooden accumulations can be easily applied by means of exclusively ground-based datasets, a combination of low altitude aerial flights (e.g. drone) and ground-based mapping (where accessible) is suggested to better resolve 3D models of larger and more complex LW accumulations in the field. Therefore, a better understanding of merged datasets is required. Solutions to the essential problem of rendering volumetric models of constitutional elements within LW accumulations from unorganized point clouds remain elusive, yet we have shown how critical advances can be exploited.

The comparison of simple models from the Pix4D volume tool (2.5D) and the PSR (3D) algorithm in MeshLab – relative to geometrically determined benchmarks - revealed that the 3D approach using PSR provided the most accurate results for LW accumulation assessment. The 2.5D models consistently overestimated the volume, by an average of 28.2%; the 3D models deviated by 6.3% (absolute) on average, with a mix of over- and under-estimation. Overestimation of accumulation volumes was expected from 2.5D models, as they include interstitial space within the accumulation. We found that for an accurate generation of a 3D mesh model, a higher number of oblique and nadir images is required, than for conventional 2.5D mesh models. Occluded geometry in the models introduced the problem of mesh closure; software algorithms must estimate this closure in sparse regions of the point cloud, often resulting in strong distortions of the resultant volume model.

Using the difference between the 2.5D and 3D volumes as a measure of deposit void space, the introduced methodology provides a consistent and objective measure for assessing void space in the field. Our results showed void proportions of 7.7 to 52.3%; these measurements showed good consistency with the results based on consideration of geometric primitive models of void space.

We successfully computed high quality 3D models of miniature LW structures along with OFM, in a controlled laboratory environment, and extracted precise accumulation volumes for the first time. Our results demonstrated the capability of this SfM methodology, which provides major advances for LW accumulation assessment in the field as well as in the laboratory. This may be of further fundamental importance for prototype accumulation models (2D, 2.5D and 3D) in hydraulic engineering using numerical modelling. For instance, mesh generation techniques will be useful for the estimation of obstructed cross-sectional area of LW accumulations and surface roughness, which affect hydraulic flow behaviour and backwater effects, respectively.

Some challenges arise for future work, including (i) properly resolving intersecting elements, especially in the accumulation centre, (ii) mesh closure processes, without losing important surface details, and (iii) assessing the effects of point sub-sampling on model quality, in order to deploy SfM photogrammetry as an effective surveying tool. Thus, progress in point cloud processing, editing and meshing algorithms is imperative, in order to generate more reliable and robust models. The workflow should be able to counter problems with rendering mesh (e.g. noise reduction, correct point normal estimation), resolving surface texture (e.g. mesh closing, recognition of void spaces) and mitigating environmental noise (e.g. shades, reflections, water surfaces), using standard camera devices such as smartphones or action cameras.

This workflow will contribute to a better understanding of LW accumulations in fluvial environments by providing parameters for accumulation volume and porosity, which are known to affect channel hydraulics and bedload processes. Such indicators can facilitate hydraulic studies and help to better assess LW accumulations in rivers. Apart from volume and porosity estimates, our method can provide significant information about constitutional materials of the accumulation, surface structure (roughness elements), log alignment and geometries, which are all crucial parameters for studying formation processes of LW accumulations. This understanding will allow for the identification of critical 'key-logs', which are responsible for jam initiation, computation of the resulting hydraulic discharge behaviour, and estimation of the effects on channel morphology in the presence of LW accumulations.

Declaration of Competing Interest

The authors declare that they have no known competing financial interests or personal relationships that could have appeared to influence the work reported in this paper.

References

Abbe, T.B., Montgomery, D.R., 1996. Large woody debris jams, channel hydraulics and habitat formation in large rivers. Regulat. Riv. Res. Manage. 12, 201–221.
Abbe, T.B., Montgomery, D.R., 2003. Patterns and processes of wood debris accumulation in the Queets river basin, Washington. Geomorphology 51, 81–107.
Acuna, M., Sosa, A., 2019. Automated volumetric measurements of truckloads through multi-view photogrammetry and 3D reconstruction software. Croatian J. For. Eng. J.

Theory Appl. For. Eng. 40, 151–162.
AGISOFT LLC RUSSIA 2018. PhotoScan - photogrammetric processing of digital images and 3D spatial data generation.
Alidoost, F., & Arefi, H., 2017. Comparison of Uas-Based Photogrammetry Software for 3d Point Cloud Generation: A Survey over a Historical Site. ISPRS Annals of Photogrammetry, Remote Sensing and Spatial Information Sciences, IV-4/W4, 55-61.
Allen, J.B., Smith, D.L., 2012. Characterizing the impact of geometric simplification on large woody debris using CFD. Int. J. Hydraulic Eng. 1, 1–14.
Alonzo, M., Andersen, H.-E., Morton, D., Cook, B., 2018. Quantifying boreal forest structure and composition using UAV structure from motion. Forests 9, 119.
Alratrout, A., Blunt, M.J., Bijeljic, B., 2018. Wettability in complex porous materials, the mixed-wet state, and its relationship to surface roughness. Proc. Natl. Acad. Sci. U.S.A. 115, 8901–8906.
Anderson, B.G., Rutherfurd, I.D., Western, A.W., 2006. An analysis of the influence of riparian vegetation on the propagation of flood waves. Environ. Modell. Software 21, 1290–1296.
ASTRE, H. 2015. SfMtoolkit, available at: http://www.visual-experiments.com/demos/sfmtoolkit/.
AUTODESK FUSION 360 2018. Integrated CAD, CAM and CAE software - Autodesk Fusion 360. https://www.autodesk.com/products/fusion-360/overview.
AUTODESK RECAP 2019. ReCap 3D - Create accurate 3D models with reality capture by Autodesk. https://www.autodesk.com/products/recap/overview.
Balaguer-Puig, M., Marques-Mateu, A., Lerma, J.L., Ibanez-Asensio, S., 2017. Estimation of small-scale soil erosion in laboratory experiments with Structure from Motion photogrammetry. Geomorphology 295, 285–296.
Benda, L.E., Sias, J.C., 2003. A quantitative framework for evaluating the mass balance of in-stream organic debris. For. Ecol. Manage. 172, 1–16.
Berger, M., Tagliasacchi, A., Seversky, L., Alliez, P., Guennebaund, G., Levine, J., Scharf, A., Silva, C., 2017. A survay of surface reconstruction from point clouds. Comput. Graph. Forum 36, 301–329.
Berger, M., Tagliasacchi, A., Seversky, L., Alliez, P., Levine, J., Scharf, A., Silva, C., 2014. State of the art in surface reconstruction from point clouds. Eurograph. Star Rep. 1, 161–185.
Bertin, S., Friedrich, H., Delmas, P., Chan, E., Gimel'Farb, G., 2015. Digital stereo photogrammetry for grain-scale monitoring of fluvial surfaces: Error evaluation and workflow optimisation. ISPRS J. Photogramm. Remote Sens. 101, 193–208.
Bianco, S., Ciocca, G., Marelli, D., 2018. Evaluating the performance of structure from motion pipelines. J. Imag. 4, 98.
Bilby, R., 1984. Removal of woody debris may affect stream channel stability. J. Forest 609–613.
Bocchiola, D., Catalano, F., Menduni, G., Passoni, G., 2002. An analytical–numerical approach to the hydraulics of floating debris in river channels. J. Hydrol. 269, 65–78.
BOIVIN, M. & BUFFIN-Bélanger, T. 2010. Using a terrestrial lidar for monitoring of large woody debris jams in gravel-bed rivers. 7th Gravelbed Rivers Conference, 5-10 September 2010, Tadoussac, Quebec, Canada (poster).
Boivin, M., Buffin-Bélanger, T., Piégay, H., 2015. The raft of the Saint-Jean River, Gaspé (Québec, Canada): a dynamic feature trapping most of the wood transported from the catchment. Geomorphology 231, 270–280.
Bretar, F., Arab-Sedze, M., Champion, J., Pierrot-Deseilligny, M., Heggy, E., Jacquemoud, S., 2013. An advanced photogrammetric method to measure surface roughness: application to volcanic terrains in the Piton de la Fournaise, reunion Island. Remote Sens. Environ. 135, 1–11.
Brown, A., Mcbroom, M., zhang, Y., 2014. Developing a Large Woody Debris Budget for the Lower San Antonio River. Texas Water Development Board, 258.
Carrivick, J.L., Smith, M.W., Quincey, D.J., 2016. Structure from Motion in the Geosciences. John Wiley & Sons, Ltd, pp. 206.
Cave, M., Davies, N., Langford, J. 2017. Cyclone Cook Slash Investigation 2017 Report. Gisborne District Council - Land and Soil Environmental Services and Protection, 121.
Chandler, J., Lane, S.N., Ashmore, P., 2000. Measuring river-bed and flume morphology and parameterising bed roughness with a Kodak DCS460 digital camera. International Archives of Photogrammetry and Remote Sensing, XXXIII, pp. 250–257.
Chen, S., Tian, D., Feng, C., Fellow, V., Kovacevi˘ C.J. 2017. Fast Resampling of 3D Point Clouds via Graphs.
Cignoni, P., Callieri, M., Corsini, M., Dellepiane, M., Ganovelli, F., Ranzuglia, G., 2008. MeshLab: an open-source mesh processing tool. In Proceedings of the 2008 Eurographics Italian Chapter Conference.
CLOUDCOMPAREV2 2016. CloudCompare V2, Version 2.6.3, Windows 64-bits.
Collins, B.D., Montgomery, D.R., Haas, A.D., 2002. Historical changes in the distribution and functions of large wood in Puget Lowland rivers. Can. J. Fish. Aquat. Sci. 59, 66–76.
Colomina, I., Molina, P., 2014. Unmanned aerial systems for photogrammetry and remote sensing: a review. ISPRS J. Photogramm. Remote Sens. 92, 79–97.
Colvard, J.R., 1998. Jamming in Yellowstone: Mapping Lagre Woody Debris in America's first National Park. Master's Thesis on the Graduate School-NEw Brunswick Rutgers, The State University of New Jersey, 60.
Cordova, J.M., Rosi-Marshall, E.J., Yamamuro, A.M., Lamberti, G.A., 2006. Quantity, controls and functions of large woody debris in Midwestern USA streams. River Res. Appl. 13.
Costabile, P., Macchione, F., 2015. Enhancing river model set-up for 2-D dynamic flood modelling. Environ. Modell. Software 67, 89–107.
Cunliffe, A.M., Brazier, R.E., Anderson, K., 2016. Ultra-fine grain landscape-scale quantification of dryland vegetation structure with drone-acquired structure-from-motion photogrammetry. Remote Sens. Environ. 183, 129–143.
Curran, J.C., Tan, L., 2010. An investigation of bed armoring processes and the formation of microclusters. Joint Federal Interagency Conference, Las Vegas, 2, 12.
Demarsin, K., Vanderstraeten, D., Volodine, T., Roose, D., 2007. Detection of closed sharp edges in point clouds using normal estimation and graph theory. Comput. Aided Des. 39, 276–283.
Dikovski, B., Lameski, P., Zdraveski, E., Kulakov, A., 2014. Structure from motion obtained from low quality images in indoor environment. Conference Paper – Vitola, Macedonia, 4.
Dixon, S.J., 2016. A dimensionless statistical analysis of logjam form and process. Ecohydrology 9, 1117–1129.
Dixon, S.J., Sear, D.A., 2014. The influence of geomorphology on large wood dynamics in a low gradient headwater stream. Water Resour. Res. 50, 9194–9210.
Eltner, A., Kaiser, A., Castillo, C., Rock, G., Neugirg, F., Abellan, A., 2016. Image-based surface reconstruction in geomorphometry – merits, limits and developments. Earth Surf. Dyn. 4, 359–389.
Fan, L., Atkinson, P.M., 2019. An iterative coarse-to-fine sub-sampling method for density reduction of terrain point clouds. Remote Sens. 11, 947.
Fausch, K.D., Northcote, T.G., 1992. Large woody debris and salmonid habitat in a small coastal british columbia stream. Can. J. Fish. Aquat. Sci. 49, 682–693.
Fetherston, K.L., Naiman, R.J., Bilby, R.E., 1995. Large woody debris, physical process, and riparian forest development in montane river networks of the Pacific Northwest. Geomorphology 13, 133–144.
Filippelli, S.K., Lefsky, M.A., Rocca, M.E., 2019. Comparison and integration of lidar and photogrammetric point clouds for mapping pre-fire forest structure. Remote Sens. Environ. 224, 154–166.
Fuhrmann, S., Goesele, M., 2011. Fusion of Depth Maps with Multiple Scales. The definitive version was published in ACM Transactions on Graphics, 30, 8.
Gasser, E., Schwarz, M., Simon, A., Perona, P., Phillips, C., Hübl, J., Dorren, L., 2019. A review of modeling the effects of vegetation on large wood recruitment processes in mountain catchments. Earth Sci. Rev. 194, 350–373.
Giirsoy, H. N. & Patrikalakis, N.M. 1992. An Automatic Coarse and Fine Surface Mesh Generation Scheme Based on Medial Axis Transform: Part I Algorithms Engineering with Computers 8, 121–137.
Gippel, C., O'Neill, I., Finlayson, B., Schantz, I., 1996. Hydraulic guidelines for the reintroduction and management of large woody debris in lowland rivers. Regul. Riv. Res. Manage. 12, 223–236.
Golbach, F., Kootstra, G., Damjanovic, S., Otten, G., van de Zedde, R., 2015. Validation of plant part measurements using a 3D reconstruction method suitable for high-throughput seedling phenotyping. Mach. Vis. Appl. 27, 663–680.
Gregory, K.J., Gurnell, A.M., Hill, C.T., 1985. The permanence of debris dams related to river channel processes. Hydrol. Sci. J. 30, 371–381.
Grigillo, D., Vrečko, A., Mikoš, M., Gvozdanović, T., Anžur, A., Vezočnik, R., Petrovič, D., 2015. Determination of large wood accumulaton in steep forested torrent using laser scanning. Eng. Geol. Soc. Territory 3, 127–130.
Gschnitzer, T., Gems, B., Mazzorana, B., Aufleger, M., 2017. Towards a robust assessment of bridge clogging processes in flood risk management. Geomorphology 279, 128–140.
Guerrero, P., Kleiman, Y., Ovsjanikov, M., Mitra, N. J. 2018. PCPNET Learning Local Shape Properties from Raw Point Clouds. Eurographics 2018 proceedings, 11.
Gupta, S.K., Shukla, D.P., 2017. 3D reconstruction of a landslide by application of UAV and Structure from Motion. AGILE 2017 – Wageningen, 7.
Gurnell, A.M., Piegay, H., Swanson, F.J., Gregory, S.V., 2002. Large wood and fluvial processes. Freshw. Biol. 47, 601–619.
Hackenberg, J., Spiecker, H., Calders, K., Disney, M., Raumonen, P., 2015. SimpleTree—An efficient open source tool to build tree models from TLS clouds. Forests 6, 4245–4294.
Harmon, M.E., Franklin, J.F., Swanson, F.J., Sollins, P., Gregory, S.V., Lattin, J.D., Anderson, N.H., Cline, S.P., Aumen, N.G., Sedell, J.R., Lienkaemper, G.W., Cromack, K., Cummins, K.W., 1986. Ecology of coarse woody debris in temperate ecosystems. Adv. Ecol. Res. 15, 133–302.
Heede, B.H., Forest, R.M., Station, R., E., 1972. Flow and channel characteristics of two high mountain streams, Rocky Mountain Forest and Range Experiment Station, Forest Service, U.S. Dept. of Agriculture.
Hétroy-Wheeler, F., Casella, E., Boltcheva, D., 2016. Segmentation of tree seedling point clouds into elementary units. Int. J. Remote Sens. 37, 2881–2907.
Hoppe, H., Derose, T., Duchamp, T., McDonald, J., Stuetzle, W., 1992. Surface reconstruction from unorganized points. ACM Siggraph, New York, pp. 71–78.
Hornbeck, J.W., Adams, M.B., Corbett, E.S., Verry, E.S., Lynch, J.A., 1993. Long-term impacts of forest treatments on water yield: a summary for northeastern USA. J. Hydrol. 150, 323–344.
Jacobson, A., Kavan, L., Sorkine-Hornung, O., 2013. Robust inside-outside segmentation using generalized winding numbers. ACM Trans. Graph. 32, 1.
Javernick, L., Brasington, J., Caruso, B., 2014. Modeling the topography of shallow braided rivers using Structure-from-Motion photogrammetry. Geomorphology 213, 166–182.
Jugie, M., Gob, F., Virmoux, C., Brunstein, D., Tamisier, V., le Coeur, C., Grancher, D., 2018. Characterizing and quantifying the discontinuous bank erosion of a small low energy river using Structure-from-Motion Photogrammetry and erosion pins. J. Hydrol. 563, 418–434.
Kaiser, A., Neugirg, F., Rock, G., Müller, C., Haas, F., Ries, J., Schmidt, J., 2014. Small-scale surface reconstruction and volume calculation of soil erosion in complex moroccan gully morphology using structure from motion. Remote Sens. 6, 7050–7080.
Kazhdan, M., Bolitho, M., Hoppe, H., 2006. Poisson Surface Reconstruction. Eurographics Symposium on Geometry Processing, 10.
Kazhdan, M., Hoppe, H., 2013. Screened poisson surface reconstruction. ACM Trans. Graph. 32, 1–13.
Keller, E., Swanson, F.J., 1979. Effects of large organic material on channel form and fluvial processes. Earth Surf. Proc. Land. 4, 361–380.
Kimme, C., Ballard, D., Sklansky, J., 1975. Finding circles by an array of accumulators.

Commun. ACM 18, 120–122.
KNAUSS, J. 1995. Von der oberen zur unteren Isar, Versuchsanst. für Wasserbau und Wasserwirtschaft, Oskar-v.-Miller-Inst.
Kraaijenbrink, P.D.A., Shea, J.M., Pellicciotti, F., Jong, S.M.D., Immerzeel, W.W., 2016. Object-based analysis of unmanned aerial vehicle imagery to map and characterise surface features on a debris-covered glacier. Remote Sens. Environ. 186, 581–595.
Lai, Y.G., 2016. Quantitative Modeling Tools for Large Woody Debris and Other In-Stream Structures. Reclamation - Managing Water in the West, 159.
Lane, S.N., Westaway, R.M., Hicks, D.M., 2003. Estimation of erosion and deposition volumes in a large, gravel-bed, braided river using synoptic remote sensing. Earth Surf. Proc. Land. 28, 249–271.
Lassettre, N.S., Kondolf, G.M., 2012. Large woody debris in urban stream channels: re-defining the problem. River Res. Appl. 28, 1477–1487.
Li, W., Bertin, S., Friedrich, H., 2018a. Combining Structure from Motion and close-range stereo photogrammetry to obtain scaled gravel bar DEMs. Int. J. Remote Sens. 39, 9269–9293.
Li, W., Guo, Q., Tao, S., Su, Y., 2018b. VBRT: a novel voxel-based radiative transfer model for heterogeneous three-dimensional forest scenes. Remote Sens. Environ. 206, 318–335.
Lienkaemper, G.W., Swanson, F.J., 1987. Dynamics of large woody debris in streams in old-growth douglas-fir forests. Can. J. For. Res. 17, 150–156.
Livers, A., Lininger, K., Kramer, N., Wohl, E., 2015. Porosity Problems. Proceedings of Wood in World Rivers Conference, Padova, Italy, June 2015.
Lobos, C., Rojas-Moraleda, R., 2013. FROM SEGMENTED MEDICAL IMAGES TO SURFACE AND VOLUME MESHES, USING EXISTING TOOLS AND ALGORITHMS. In VI International Conference on Adaptive Modeling and Simulation ADMOS 2013, 12.
Lucia, A., Schwientek, M., Eberle, J., Zarfl, C., 2018. Planform changes and large wood dynamics in two torrents during a severe flash flood in Braunsbach, Germany 2016. Sci. Total Environ. 640–641, 315–326.
Maiti, A., Chakravarty, D., 2016. Performance analysis of different surface reconstruction algorithms for 3D reconstruction of outdoor objects from their digital images. Springerplus 5, 932.
Mancini, F., Dubbini, M., Gattelli, M., Stecchi, F., Fabbri, S., Gabbianelli, G., 2013. Using unmanned aerial vehicles (UAV) for high-resolution reconstruction of topography: the structure from motion approach on coastal environments. Remote Sens. 5, 6880–6898.
Manners, R.B., Doyle, M.W., 2008. A mechanistic model of woody debris jam evolution and its application to wood-based restoration and management. River Res. Appl. 24, 1104–1123.
Martin, D.J., Harden, C.P., Tran, L., Opavlowsky, R.T., 2018. Investigating patterns of in-channel wood deposition locations in a low gradient, variably-confined alluvial river system. Prog. Phys. Geogr. 42 (2), 139–161.
Martin, W.N., Aggarwal, J.K., 1983. Volumetric descriptions of objects from multiple views. In IEEE TRANSACTIONS ON PATTERN ANALYSIS AND MACHINE INTELLIGENCE,, PAMI-5,, pp. 150–158.
Mazzorana, B., Fuchs, S., 2010. Fuzzy formative scenario analysis for woody material transport related risks in mountain torrents. Environ. Modell. Softw. 25, 1208–1224.
Megahan, W.F., Nowlin, R.A., 1976. Sediment storage in channels draining small forested watersheds in the mountains of central Idaho. v. 1976, 245100.
Micheletti, N., Chandler, J.H., Lane, S.N., 2015. Investigating the geomorphological potential of freely available and accessible structure-from-motion photogrammetry using a smartphone. Earth Surf. Proc. Land. 40, 473–486.
Milan, D.J., Heritage, G.L., Hetherington, D., 2007. Application of a 3D laser scanner in the assessment of erosion and deposition volumes and channel change in a proglacial river. Earth Surf. Proc. Land. 32, 1657–1674.
Mitra, N.J., Nguyen, A., 2003. Estimating surface normals in noisy point cloud data. Symposium on Computational Geometry, pp. 1–7.
Moos, C., Bebi, P., Schwarz, M., Stoffel, M., Sudmeier-Rieux, K., Dorren, L., 2018. Ecosystem-based disaster risk reduction in mountains. Earth Sci. Rev. 177, 497–513.
Morel, J., Bac, A., Véga, C., 2018. Surface reconstruction of incomplete datasets: a novel poisson surface approach based on CSRBF. Comput. Graph. 74, 44–55.
Morgan, J.A., Brogan, D.J., Nelson, P.A., 2016. Application of structure-from-motion photogrammetry in laboratory flumes. Geomorphology 276, 125–143.
Mosbrucker, A.R., Major, J.J., Spicer, K.R., Pitlick, J., 2017. Camera system considerations for geomorphic applications of SfM photogrammetry. Earth Surf. Proc. Land. 42, 969–986.
Mosley, M.P., 1981. The influence of organic debris on channel morphology and bedload transport in a New Zealand forest stream. Earth Surf. Proc. Land. 6, 571–579.
Mostegel, C., Rumpler, M., 2012. Robust Surface Reconstruction from Noisy Point Clouds using Graph Cuts. Inst. for Computer Graphics and Vision Graz University of Technology, Austria, pp. 56.
Nakamura, F., Swanson, F.J., 1994. Distribution of coarse woody debris in a mountain stream, western Cascade Range, Oregon. Can. J. Fish. Aquat. Sci. 24, 9.
Nocerino, E., Lago, F., Morabito, D. R., F., Porzi, L., Poiesi, F., Rota Bulo, S., Chippendale, P., Locher, A., Havlena, M., Van Gool, L., Eder, M., Foetschl, A., Hilsmann, A., Kausch, L. & Van Gool, L. 2017. A smartphone-based 3D pipeline for the creative industry - The replicate eu project -. 3D VIRTUAL RECONSTRUCTION AND VISUALIZATION OF COMPLEX ARCHITECTURES, 42 (W3), 535-541.
Nurunnabi, A., Sadahiro, Y. & Lindenbergh, R., 2017. Robust Cylinder Fitting in Three-Dimensional Point Cloud Data. ISPRS - International Archives of the Photogrammetry, Remote Sensing and Spatial Information Sciences, XLII-1/W1, pp. 63–70.
Orru, C., Blom, A., Chavarrias, V., Ferrara, V., Stecca, G., 2016. A new technique for measuring the bed surface texture during flow and application to a degradational sand-gravel laboratory experiment. Water Resour. Res. 52, 7005–7022.
Pagliara, S., Carnacina, I., 2010. Temporal scour evolution at bridge piers: effect of wood debris roughness and porosity. J. Hydraul. Res. 48, 3–13.
Peterson, E.B., Klein, M., Stewart, R.L., 2015. Whitepaper on Structure from Motion (SfM) Photogrammetry: Constructing Three Dimensional Models from Photography. Reclamation - Managing Water in the West, 47.
Phillips, C., Marden, M., Basher, L.R., 2018. Geomorphology and forest management in New Zealand's erodible steeplands: an overview. Geomorphology 307, 107–121.
Piegay, H., 1993. Nature mass and preferential sites of coase woody debirs deposition in the lower ain valley (Mollon Reach), france. Regul. Rivers Res. Manage. 8, 359–372.
PIX4D SWITZERLAND 2018. Pix4Dmapper Pro - Educational, Version 4.1.25.
PIX4DMAPPER 2018. Pix4Dmapper 4.1 - User Manual. 305.
Raumonen, P., Kaasalainen, M., Åkerblom, M., Kaasalainen, S., Kaartinen, H., Vastaranta, M., Holopainen, M., Disney, M., Lewis, P., 2013. Fast automatic precision tree models from terrestrial laser scanner data. Remote Sens. 5, 491–520.
Ravazzolo, D., Mao, L., Picco, L., Lenzi, M.A., 2015. Tracking log displacement during floods in the Tagliamento River using RFID and GPS tracker devices. Geomorphology 228, 226–233.
Remondino, F., 2003. From point cloud to surface the modeling and visulization problem. International Archives of the Photogrammetry, Remote Sensing and Spatial Information Sciences, XXXIV-5/W10, 11.
Rigon, E., Comiti, F., Mao, L., Lenzi, M. A., 2008. Relationships among basin area, sediment transport mechanisms and wood storage in mountain basins of the Dolomites (Italian Alps). Monitoring, Simulation, Prevention and Remediation of Dense Debris Flows Ii, 60, 163–172.
Rodriguez-Galiano, V.F., Ghimire, B., Rogan, J., Chica-Olmo, M., Rigol-Sanchez, J.P., 2012. An assessment of the effectiveness of a random forest classifier for land-cover classification. ISPRS J. Photogramm. Remote Sens. 67, 93–104.
Ruiz-Villanueva, V., Bladé, E., Sánchez-Juny, M., Marti-Cardona, B., Díez-Herrero, A., Bodoque, J.M., 2014. Two-dimensional numerical modeling of wood transport. J. Hydroinf. 16, 1077–1096.
Ruiz-Villanueva, V., Piegay, H., Gaertner, V., Perret, F., Stoffel, M., 2016. Wood density and moisture sorption and its influence on large wood mobility in rivers. Catena 140, 182–194.
Ruiz-Villanueva, V., Wyżga, B., Mikuś, P., Hajdukiewicz, M., Stoffel, M., 2017. Large wood clogging during floods in a gravel-bed river: the Długopole bridge in the Czarny Dunajec River, Poland. Earth Surf. Proc. Land. 42, 516–530.
Rusyda, M.I., 2014. Woody debris jam formation by obstructions in river-floodplain systems during floods. Department of Urban and Environmental Engineering - Kyushu University, Fukuoka, Japan, Doctoral Thesis, 136.
Ružić, I., Marović, I., Benac, Č., Ilić, S., 2014. Coastal cliff geometry derived from structure-from-motion photogrammetry at Stara Baška, Krk Island, Croatia. Geo-Mar. Lett. 34, 555–565.
Sanhueza, D., Picco, L., Ruiz-Villanueva, V., Iroumé, A., Ulloa, H., Barrientos, G., 2019. Quantification of fluvial wood using UAVs and structure from motion. Geomorphology 345, 106837.
Scaioni, M., Feng, T., Lu, P., Qiao, G., Tong, X., Li, R., Barazzetti, L., Previtali, M., Roncella, R. 2015. Closerange photogrammetric techniques for deformation measurement: Applications to landslides. Modern technologies for landslide monitoring and prediction, pp. 13–41.
Schalko, I., Schmocker, L., Weitbrecht, V., Boes, R., 2016. Backwater rise due to driftwood accumulation. Interpraevent 2016, 628–637.
Schalko, I., Schmocker, L., Weitbrecht, V., Boes, R.M., 2018. Backwater rise due to large wood accumulations. J. Hydraul. Eng. 144, 04018056.
Schmocker, L., Weitbrecht, V., 2013. Driftwood: Risk Analysis and Engineering Measures. J. Hydraul. Eng. 139, 683–695.
Schneider, F.D., Leiterer, R., Morsdorf, F., Gastellu-Etchegorry, J.-P., Lauret, N., Pfeifer, N., Schaepman, M.E., 2014. Simulating imaging spectrometer data: 3D forest modeling based on LiDAR and in situ data. Remote Sens. Environ. 152, 235–250.
Scott, D.N., Wohl, E., Yochum, S.E., 2019. Wood Jam dynamics database and assessment model (WooDDAM): a framework to measure and understand wood jam characteristics and dynamics. River Res. Appl.
Seitz, L., Haas, C., Noack, M., Wieprecht, S., 2018. From picture to porosity of river bed material using structure-from-motion with multi-view-stereo. Geomorphology 306, 80–89.
Shao, H.-C., Hwang, W.-L., Chen, Y.-C. 2018. A Coarse-to-Fine Multiscale Mesh Representation And Its Applications. Electrical Engineering and Systems Science – Image and Video Processing, 15.
Sheng, B., Zhao, F., Yin, X., Zhang, C., Wang, H., Huang, P., 2018. A lightweight surface reconstruction method for online 3D scanning point cloud data oriented toward 3D printing. Mathemat. Probl. Eng. 2018, 1–16.
Smikrud, K.M., Prakash, A., 2006. Monitoring large woody debris dynamics in the unuk river, alaska using digital aerial photography. GIScience Remote Sens. 43, 142–154.
Smith, D.L., Allen, J.B., Eslinger, O., Valenciano, M., Nestler, J., Goodwin, R.A., 2011. Hydraulic modeling of large roughness elements with computational fluid dynamics for improved realism in stream reconstruction planning. In Stream Restoration in Dynamic Fluvial Systems: Scientific Approaches, Analyses, and Tools; Geophysical Monograph Series, 194, pp. 115–123.
Smith, M.W., Carrivick, J.L., Quincey, D.J., 2016. Structure from motion photogrammetry in physical geography. Prog. Phys. Geogr. 40 (2), 247–275.
Smith, R.D., Sidle, R.C., Porter, P.E., Noel, J.R., 1993. Effects of experimental removal of woody debris on the channel morphology of a forest, gravel-bed stream. J. Hydrol. 152, 153–178.
Spreitzer, G., Tunnicliffe, J., Friedrich, H., 2019. Using structure from motion photogrammetry to assess large wood (LW) accumulations in the field. Geomorphology 346, 20.
Stumpf, A., Malet, J.P., Allemand, P., Pierrot-Deseilligny, M., Skupinski, G., 2015. Ground-based multi-view photogrammetry for the monitoring of landslide

deformation and erosion. Geomorphology 231, 130–145.
Tazir, M.L., Checchin, P., Trassoudaine, L. 2016. Color-based 3D Point Cloud Reduction. In 14th International Conference on Control, Automation, Robotics and Vision (ICARCV), pp. 1–7.
Tonon, A., Picco, L., Rainato, R., 2018. Test of methodology for developing a large wood budget: a 1-year example from a regulated gravel bed river following ordinary floods. Catena 165, 115–124.
Tonon, A., Picco, L., Ravazzolo, D., Lenzi, M.A., 2014. Using a terrestrial laser scanner to detect wood characteristics in gravel-bed rivers. J. Agric. Eng. 45, 161.
TRRP 2018. Trinity River Restoration Program. Online Webpage: "http://www.trrp.net/".
Tunnicliffe, J., Brierley, G., Fuller, I.C., Leenman, A., Marden, M., Peacock, D., 2018. Reaction and relaxation in a coarse-grained fluvial system following catchment-wide disturbance. Geomorphology 307, 50–64.
Uchiogi, T., Shima, J., Tajima, H., Ishikawa, Y., 1996. Design methods for wood-debris-entrapment. Proc. Interprevent Conf. 5, 279–288.
van Wagner, C.E., 1968. The line intersect method in forest fuel sampling. For. Sci. 14, 20–27.
Ventres-Pake, R., Nahorniak, M., Kramer, N., O'neill, J., Abbe, T. 2019. Integrating Large Wood Jams into hydraulic Models: Evaluating a Porous Plate Modeling Method. In 4th International Conference on Wood in World Rivers 2019, Valdivia, Chile.
Verma, A.K., Bourke, M.C., 2019. A method based on structure-from-motion photogrammetry to generate sub-millimetre-resolution digital elevation models for investigating rock breakdown features. Earth Surf. Dyn. 7, 45–66.
VISUALSFM 2018. VisualSFM Online platform, Available at: http://ccwu.me/vsfm/.
Vosselman, G., Gorte, B. G. H., Sithole, G. & Rabbani, T. 2004. recognising structure in laser scanner point clouds. ISPRS 2004 : proceedings of the ISPRS working group VIII/2 : laser scanning for forest and landscape assessment, University of Freiburg, pp. 33–38.
Wallerstein, N. P., Thorne, C.R. & Doyle, M.W. 1997. Spatial distribution and impact of large woody debris in northern Mississippi. Management of Landscapes Disturbed by Channel Incision, Wang SSY, Langendoen EJ, Shields FD (eds). University of Mississippi: Mississippi, USA;, 145-150.
Wang, C., Wang, Q., Meire, D., Ma, W., Wu, C., Meng, Z., van de Koppel, J., Troch, P., Verhoeven, R., de Mulder, T., Temmerman, S., 2016. Biogeomorphic feedback between plant growth and flooding causes alternative stable states in an experimental floodplain. Adv. Water Resour. 93, 223–235.
Wang, R., Peethambaran, J., Chen, D., 2018. LiDAR point clouds to 3-D Urban Models$:$ a review. IEEE J. Sel. Top. Appl. Earth Obs. Remote Sens. 11, 606–627.
Warren, W.G., Olsen, P.F., 1964. A Line intersect technique for assessing logging waste. Forest Sci. 10, 267–276.
Waske, B., Braun, M., 2009. Classifier ensembles for land cover mapping using multitemporal SAR imagery. ISPRS J. Photogramm. Remote Sens. 64, 450–457.
Webb, A.A., Erskine, W.D., 2003. Distribution, recruitment, and geomorphic significance of large woody debris in an alluvial forest stream: tonghi Creek, southeastern Australia. Geomorphology 51, 109–126.
Westoby, M.J., Brasington, J., Glasser, N.F., Hambrey, M.J., Reynolds, J.M., 2012. 'Structure-from-Motion' photogrammetry: a low-cost, effective tool for geoscience applications. Geomorphology 179, 300–314.
Widlowski, J.-L., Côté, J.-F., Béland, M., 2014. Abstract tree crowns in 3D radiative transfer models: Impact on simulated open-canopy reflectances. Remote Sens. Environ. 142, 155–175.
Williams, F., Schneider, T., Silva, C., Zorin, D., Bruna, J., Panozzo, D., 2018. Deep geometric prior for surface reconstruction. N. Y. Univ. In ArXiv 2018, 13.
Wohl, E., 2014. A legacy of absence: wood removal in US rivers. Progr. Phys. Geogr. Earth Environ. 38, 637–663.
Wohl, E., Lininger, K.B., Fox, M., Baillie, B.R., Erskine, W.D., 2017. Instream large wood loads across bioclimatic regions. For. Ecol. Manage. 404, 370–380.
Wohl, E., Scott, D.N., 2017. Wood and sediment storage and dynamics in river corridors. Earth Surf. Proc. Land. 42, 5–23.
Wolff, K., Kim, C., Zimmer, H., Schroers, C., Botsch, M., Sorkine-Hornung, O., Sorkine-Hornung, A. 2016. Point Cloud Noise and Outlier Removal for Image-Based 3D Reconstruction. pp. 118–127.
Woodget, A.S., Austrums, R., Maddock, I.P., Habit, E., 2017. Drones and digital photogrammetry: from classifications to continuums for monitoring river habitat and hydromorphology. Wiley Interdiscipl. Rev. Water 4, e1222.
Wright, A., Marcus, W.A., Aspinall, R., 2000. Evaluation of multispectral, fine scale digital imagery as a tool for mapping stream morphology. Geomorphology 33, 107–120.
Wróżyński, R., Pyszny, K., Sojka, M., Przybyła, C., Murat-Błażejewska, S., 2017. Ground volume assessment using 'Structure from Motion' photogrammetry with a smartphone and a compact camera. Open Geosci. 9.
Wyżga, B., Zawiejska, J., 2005. Wood storage in a wide mountain river: case study of the Czarny Dunajec, Polish Carpathians. Earth Surf. Proc. Land. 30, 1475–1494.
Yousefhussien, M., Kelbe, D.J., Ientilucci, E.J., Salvaggio, C., 2018. A multi-scale fully convolutional network for semantic labeling of 3D point clouds. ISPRS J. Photogramm. Remote Sens. 143, 191–204.
Yrttimaa, T., Saarinen, N., Luoma, V., Tanhuanpää, T., Kankare, V., Liang, X., Hyyppä, J., Holopainen, M., Vastaranta, M., 2019. Detecting and characterizing downed dead wood using terrestrial laser scanning. ISPRS J. Photogramm. Remote Sens. 151, 76–90.
Zhang, W., Thompson, K.E., Reed, A.H., Beenken, L., 2006. Relationship between packing structure and porosity in fixed beds of equilateral cylindrical particles. Chem. Eng. Sci. 61, 8060–8074.
Zhou, Q., Chen, Y., 2011. Generalization of DEM for terrain analysis using a compound method. ISPRS J. Photogramm. Remote Sens. 66, 38–45.
Zimmerman, R.C., Goodlett, J.C., Comer, G.H., 1967. The influence of vegetation on channel form of small streams. IAHS Publ. 75, 255–275.